

Deep drilling in the time domain with DECam II: characterizing the light curves of candidates in the extragalactic fields

Melissa L. Graham,^{1*} Midori Rollins,¹ Robert A. Knop,² Suhail Dhawan,³ Gloria Fonseca Alvarez,⁴ Christopher A. Phillips,¹ Guy Nir,² Emily Ramey,² and Peter E. Nugent²

¹*DIRAC Institute, Department of Astronomy, University of Washington, 3910 15th Avenue NE, Seattle, WA 98195, USA*

²*E.O. Lawrence Berkeley National Laboratory, 1 Cyclotron Rd., Berkeley, CA, 94720*

³*Institute of Astronomy and Kavli Institute for Cosmology, University of Cambridge, Madingley Road, Cambridge CB3 0HA, UK*

⁴*NSF NOIRLab, 950 N. Cherry Ave., Tucson, AZ 85719, USA*

Accepted XXX. Received YYY; in original form ZZZ

ABSTRACT

In this second paper on the DECam deep drilling field (DDF) program we release 2,020 optical *gri*-band light curves for transients and variables in the extragalactic COSMOS and ELAIS fields based on time series observations with a 3-day cadence from semester 2021A through 2023A. In order to demonstrate the wide variety of time domain events detected by the program and encourage others to use the data set, we characterize the sample by presenting a brief analysis of the light curve parameters such as time span, amplitude, and peak brightness. We also present preliminary light curve categorizations, and identify *potential* stellar variables, active galactic nuclei, tidal disruption events, supernovae (such as Type Ia, Type IIP, superluminous, and gravitationally lensed supernovae), and fast transients. Where relevant, the number of identified transients is compared to the predictions of the original proposal. We also discuss the challenges of analyzing DDF data in the context of the upcoming Vera C. Rubin Observatory and its Legacy Survey of Space and Time, which will include DDFs. Images from the DECam DDF program are available without proprietary period and the light curves presented in this work are publicly available for analysis.

Key words: surveys – methods: observational – techniques: image processing

1 INTRODUCTION

The term "deep drilling" refers to an astronomical survey strategy in which a specific area of sky, typically a small field or the field-of-view of the telescope being used, is observed repeatedly with high frequency ("drilled") to detect time-variable sources and to build up depth by stacking the sequence of images. This strategy is especially well-suited to explorations of the faint, fast, and high-redshift (high- z) universe of Galactic and extragalactic transients and variables.

Two of the most well known modern optical deep fields are the Hubble Deep and Ultra Deep fields. Even without the "drilling" component and just two to five epochs of observations, high- z supernovae¹ (SNe) and active galactic nuclei (AGN) were discovered and analyzed (e.g., Blakeslee et al. 2003; Sarajedini et al. 2003; Strolger et al. 2004; Strolger & Riess 2006). Ground-based time-domain surveys also began obtaining deep observations of small-area fields with low cadence (weeks or more between observations) to find high-redshift SNe (e.g., Barris et al. 2004; Poznanski et al. 2007).

The first optical multi-band time-domain survey that could be considered to employ a "deep drilling" strategy was the Supernova Legacy Survey (SNLS), which was based on the four one-square-degree Deep fields of the Canada France Hawaii Telescope (CFHT)

Legacy Survey (CFHTLS; e.g., Astier et al. 2006). At the time, the CFHTLS Deep field survey was referred to as a "rolling search" to represent how the multi-band observations were repeated frequently and continuously over the months when each of the four Deep fields was accessible. The rolling nature of the SNLS led to better characterizations for Type Ia supernova (SN Ia) light curves, especially at early times, which in turn led to more efficient use of the limited resources for spectroscopic follow-up (Sullivan et al. 2006) and better constraints on any cosmological evolution in the SN Ia light curves (Conley et al. 2006).

More recent examples of deep, well-cadenced time-domain optical imaging surveys include the Pan-STARRS1 Medium Deep Survey (Tonry et al. 2012) and the Dark Energy Survey Supernova program (DES-SN; Kessler et al. 2015). In the near future, the 10-year Legacy Survey of Space and Time (LSST) executed by the new Vera C. Rubin Observatory will include at least five deep fields with a multi-band "deep drilling" strategy, along with its wide-area time-domain coverage of the southern sky (Ivezić et al. 2019; Bianco et al. 2022). At the time of this publication the strategy had yet to be finalized, but proposals included, e.g., an hour-long series of ~ 30 second exposures for a single 9.6 deg^2 field which rotates through the *griz* filters and is repeated every 2-3 nights for a few months (Ivezić et al. 2019), or a combination of rolling surveys in ultradeep fields ($z < 1.1$) with a high cadence for a limited number of seasons and in deep fields ($z < 0.7$) with a three-night cadence every season (Gris et al. 2024). Regardless of the exact strategy adopted, the LSST deep

* E-mail: mlg3k@uw.edu

¹ Granted, high- z SNe can be found without the "drilling" component as they last for weeks to months in the rest frame and benefit from an extended visibility window thanks to cosmological time dilation.

drilling fields will provide unprecedented access to time-domain astrophysics on timescales of minutes to days, and by stacking the nightly sequences will provide access to the faint and high- z variable and transient universe.

In order to prepare for the LSST era of time domain astronomy a new deep drilling program with the Dark Energy Camera (DECam; DePoy et al. 2008) began in 2021. The survey strategy, processing pipelines, and the first two semesters of data was presented in Graham et al. (2023). In this work, we present and make a preliminary analysis of the first five semesters of data for the two extragalactic deep drilling fields (DDFs) and release 2,020 light curves in the *gri* filters. The main goal of this paper is to provide an overview of the data available, and to encourage and enable public use. In Section 2 we describe the observations and how objects were detected and measured in difference images; the construction of nightly-epoch light curves from the difference image photometry; how we cross-matched to other transient- and static-sky catalogs of the extragalactic DDFs; and where these results are publicly accessible. In Section 3 we make *preliminary* classifications for potential variables and transients, and illustrate the difference-image photometry that is available by showing a variety of representative light curves. Full photometric classification with, e.g., template fits, machine learning algorithms, or direct-image photometry is beyond the scope of this paper and left for future work. In Section 4 we conclude and describe future planned work for the DECam DDF, which restarted observations in the 2024A semester.

2 OBSERVATIONS

The overall design of the DECam DDF program and the real-time data processing pipeline is described in detail in (Graham et al. 2023, hereafter referred to as Paper I). This program began in semester 2021A and ran through 2023A, and at the time of writing was planned to start again in semester 2024A. During all semesters, the DECam DDF was executed as one of the programs of the DECam Alliance for Transients (DECAT): a group of independent time-domain programs who pool their awarded time, are co-assigned nights, and share in the observing duties to effectively run a queue service. The proprietary period has been waived for this program’s images.

As described in Paper I, the DECam DDF covered two Galactic and two extragalactic fields, COSMOS (10h, +2 deg) and ELAIS (0h, -43 deg). These extragalactic fields have been previously covered by legacy surveys across the electromagnetic spectrum. This work presents a preliminary characterization – and releases for public analysis – of difference-image light curves for objects in the two extragalactic fields over five semesters from 2021A through 2023A (whereas Paper I published only sources from 2021).

The DECam DDF observing strategy was to visit the COSMOS and/or ELAIS field once every three nights while the field was accessible (airmass < 1.5, although higher-airmass visits were done on rare occasions to fill scheduling gaps). Each visit was composed of five sequences, each of which obtained exposures at each of three (or two) adjacent pointings for COSMOS (or ELAIS): 80, 70, and 90 seconds in the *g*, *r*, and *i* filters, respectively. Each pointing thus received a total of 15 exposures per night. The limiting magnitude was approximately 23.5 mag for each filter.

Processing pipelines to perform difference-imaging, source detection and association, photometric calibration, real-bogus classification and alert production were adapted from the Dark Energy Survey pipeline (Goldstein et al. 2019b). The pipelines inputs, settings, and output photometric data products are described in full in Section 3 of

Paper I. In this work we adopt the same pipelines and data products, and use the same terminology: detections in individual difference-images are called *objects*, and objects that are within $1''$ of each other are associated into *candidates*.

It is essential to understand that the pipelines currently only consider *positive* difference-image fluxes as detected objects. This is fine for transients which do not exist in the reference images (and thus always have a positive flux in the difference image). However, for astronomical phenomena like active galactic nuclei or variable stars which can be present in the reference image and can increase or decline in brightness, creating positive or negative objects in the difference images, the candidate light curves presented here will be incomplete (i.e., missing the epochs when fainter than in the reference image).

2.1 Data Access

All images from the DECam DDF have no proprietary period and can be retrieved from the NOIRLab Astro Data Archive². The full nightly-epoch light curves and the light curve summary parameters described in Section 2.2, and the cross-match lists in Section 2.4, are all publicly available via GitHub³.

2.2 Nightly-Epoch Light Curves

Nightly-epoch light curves are created for candidates that meet data-quality thresholds, as described in Paper I. To summarize here, the first step is to reject objects with real-bogus scores of < 0.1 (79% of all objects). The second step is to reject candidates that are associated with < 10 objects (53% of all candidates), and then those which the mean real-bogus score of all of their associated (unrejected) objects is < 0.4 (52% of the remaining candidates). After these rejection steps, 2,020 candidates remain. A total of 1089 candidates are in COSMOS, and 931 are in ELAIS.

Nightly-epoch light curves are generated by grouping objects by night and filter, and calculating their mean time of observation, mean apparent difference-image magnitude, and mean real-bogus score. The magnitude error for the nightly epoch is calculated by adding in quadrature the mean of the object magnitude errors and the standard deviation in the object magnitudes. As of the end of the 2023A semester, the COSMOS field had 84 unique epochs and ELAIS had 97. We also estimate a nightly-epoch limiting magnitude by combining the 5σ detection limits as measured in the individual processed CCD images for each filter on the given night (Paper I).

We use the term “lonely epochs” to refer to nightly epochs for a given candidate that have a mean real-bogus score of < 0.4 and no other nightly-epoch within 14 days that has a mean real-bogus score of > 0.4. Nightly epochs that are flagged as “lonely epochs” are not included when calculating the light curve summary parameters (below) because they are more likely to be spurious or unassociated with the true astrophysical transient. This use of “lonely epoch” flags is new, and was not done in Paper I.

We calculate four parameters to represent the main characteristics of the nightly-epoch light curves: the minimum difference-image magnitude (brightest epoch); the amplitude (maximum minus minimum difference-image magnitude); time span (days between the

² <https://noirlab.edu/public/projects/astrodataarchive/>

³ Find all the data for this paper in the directory `transients_science` within the repository at https://github.com/MelissaGraham/decam_ddf_tools

first and last difference-image detection); and number of non-lonely epochs. These four parameters are determined for each filter individually (g , r , and i) and over all filters.

In Figures 1 and 2 we show the histograms of the nightly-epoch light curve parameters, and scatter plots of their relations with each other. Some quantization in time span is seen in the COSMOS field, which has shorter seasons from CTIO due to its more equatorial declination. Dotted lines at the anticipated (theoretical) limiting magnitude of the science (direct) images, ~ 23.5 mag in each filter (Section 2; Paper I), are drawn for plots which have an axis of minimum magnitude. This addition demonstrates that the faintest difference-image detections align with the survey’s limit. It is these nightly-epoch light curves and their summary parameters that are used as the starting point of our analysis in Section 3.

2.3 Transient-Sky Counterparts

As there are many all-sky surveys detecting and reporting transients, we use the Transient Name Server⁴ to compile a list of classified transients that occurred in the COSMOS or ELAIS field in the last three years. We found five within the field boundaries, only one of which happened while our program was observing: SN 2023dyl, a Type Ia supernova, was detected as DC23klgla. However, since our program only detected five epochs in i -band and one in g -band, this particular candidate did not make it on to the list of potential SN Ia that is discussed in Section 3.5.

2.4 Static-Sky Counterparts

To identify static-sky counterparts (stars and host galaxies) we cross-match our DECAM DDF candidates to the Tractor Catalog from Data Release 10 (DR10) of the DESI Legacy Imaging Surveys⁵ (Dey et al. 2019). We perform the cross-matching in the JupyterLab environment at the Astro Data Lab at NSF’s National Optical-Infrared Astronomy Research Laboratory (NOIRLab), using their `queryClient` service.

We start by simply counting the number of Tractor objects within a radius of $72''$ (0.02°) as a basic check that the catalog does cover the location of the candidate. Since the locations of the DECAM DDF were chosen, in part, based on past DECAM coverage the expectation was that all candidates’ coordinates would be covered by the Tractor catalog. We confirmed this to be the case: there are 100 to 600 Tractor objects within a radius of 0.02° of each of our candidates.

We then used the `SkyCoord` class in the `astropy` package to calculate the separation distance between each candidate and the Tractor objects within a radius of 0.02° . If the nearest Tractor object had a `type` equal to `PSF` (i.e., a star), and it was within two times the size of the r -band point-spread function (PSF; column `psfsize_r`), then the candidate was flagged as being cross-matched with a star. If the nearest Tractor object was not a star but an extended object, and the separation distance was less than five times the object’s half-light radius, then the candidate was flagged as being cross-matched to a potential host galaxy.

Of the 2,020 candidates, 1081 (53%) were matched to a star, 802 (40%) were matched to a potential host galaxy, and 137 (7%) had no match. Of the 802 candidates that were matched to a potential host galaxy, 619 (77%) were flagged as potentially nuclear because the separation distance was less than the PSF size. These potentially

nuclear candidates might be, e.g., transients in the cores of their host galaxy or active galactic nuclei (AGN).

Of the 1081 candidates cross-matched to a star, 477 (44%) were also within 5 half-light radii of the nearest extended object. Of the 802 candidates cross-matched to a galaxy, 93 (12%) were also within 2 times the PSF of the nearest star. These candidates were flagged for being potentially mis-matched.

For all cross-matched objects we retained the following columns from the DR10 Tractor catalog⁶: Right Ascension and Declination coordinates (columns `ra` and `dec`); Milky Way E(B-V) value (`ebv`, Schlegel et al. 1998); the Legacy Survey’s unique identifier (`ls_id`); apparent magnitudes in filters g , r , and i (`mag_g`, `mag_r`, `mag_i`); the best-fit model type (PSF; round exponential galaxy model, `REX`; de Vaucouleurs model, `DEV`; exponential model, `EXP`; or a Sersic model, `SER`); ellipticity parameters (`shape_e1` and `shape_e2`); the half-light radius (`shape_r`); the sersic index (`sersic`); and the PSF size in filters g , r , and i (`psfsize_g`, `psfsize_r`, `psfsize_i`).

For candidates cross-matched with a potential host galaxy, we use a radius of $2''$ to cross-match the potential host to the objects in the DR9 Tractor and photometric redshift (`photo-z`) catalogs. This step of cross-matching the DR10 and DR9 Tractor catalogs was necessary as the `photo-z` were only available with DR9. The use of $2''$ is appropriate in this case because we are not cross-matching the *transient* to the potential host galaxies in the DR9 Tractor catalog, but cross-matching between galaxy central coordinates. We find that 92% of the potential host galaxies have a photometric redshift, and that of these, 15% also have a spectroscopic redshift. From the DR9 Tractor and `photo-z` catalogs we retain the columns of mean and standard deviation of the `photo-z` posterior distribution function (`PDF`; `z_phot_mean` and `z_phot_std`), as well as the spectroscopic redshift (`z_spec`).

In Figure 3 we provide some plots to illustrate the cross-matched population from the DR10 and DR9 Tractor catalogs. At upper left, histograms of the matched object sizes for stars show a range of PSF FWHM from about $1''$ to $2''$. The distribution of PSF size is bimodal, and further investigation (not shown) revealed this to come from only the ELAIS field. Since the PSF sizes are actually the weighted average of the PSF FWHM in a given band and not measured from the source directly, this bimodality represents the image quality (seeing) distribution of the survey in the ELAIS region. The size distribution for potential host galaxies has many more small half-light radii ($< 2''$) than larger extended objects, but this is expected as the candidates themselves are more likely to be intermediate to high redshift, or active AGN with bright cores. At upper right, the histogram of the separation distances for cross-matched stars and galaxies exhibits a similar slope on the small-separation end. There is an excess of candidates with a separation distance of $\sim 2''$ from cross-matched stars and, to a lesser degree, galaxies. The bimodality in the separation distribution exists for both COSMOS and ELAIS, and is unrelated to the bimodality in the distribution of PSF size seen at upper left (i.e., there is no correlation between separation and PSF size for matched stars). To test if it was due to chance associations we generated 1000 random coordinates in the ELAIS and COSMOS fields, applied the same cross-match process, and found that the distribution of separations for coincidental matches peaked at $\sim 2''$. The excess number of matched stars is ~ 60 , or about 3% of the total number of candidates (although it does look oversized in the log-log plot). The static-sky matched objects are used for context in Section 3, but none of our

⁴ <https://www.wis-tns.org/>

⁵ <https://www.legacysurvey.org>

⁶ For more information about the columns, see <https://www.legacysurvey.org/dr10/catalogs/>.

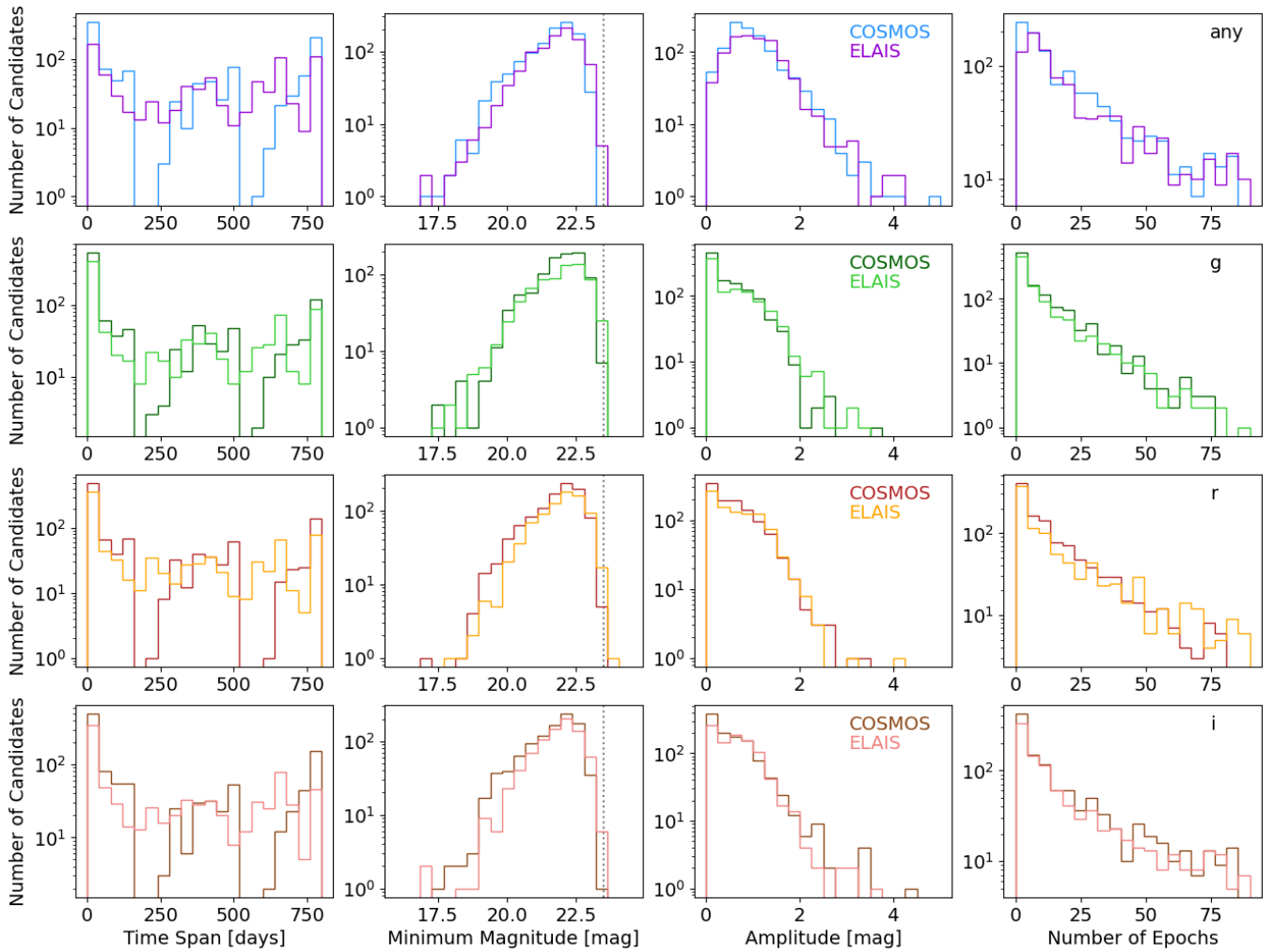


Figure 1. Histograms for the nightly-epoch light curve parameters of all 2,020 candidates that passed data-quality cuts.

results depend strongly on it, so we find this amount of contamination acceptable.

In the lower-left panel of Figure 3 we plot the half-light radius versus the separation for candidates with potential host galaxies, with point styles representing the best-fit extended-source models. This panel gives an overall impression of the number of potential hosts with the different profiles, and shows that candidates with more significant offsets ($> 2''$) are typically in galaxies with de Vaucouleurs or exponential profiles. This panel also shows a distinct group of matched objects that are best-fit with Sérsic profiles, and have separations of $2''$. The static-sky matched objects are used for context in Section 3, but none of our results depend strongly on it. Finally, in the lower-right panel of Figure 3 we show the histograms of photometric and spectroscopic redshifts for potential host galaxies. Although the two distributions do have similar shapes, the distribution of spec- z is shifted towards lower redshifts and a Kolmogorov-Smirnov test shows that they are not representative of the same underlying distribution (i.e., are significantly different, as expected).

2.5 Spectroscopic Counterparts

We also cross-matched to the early data release of the Dark Energy Spectroscopic Instrument, DESI (DESI Collaboration et al. 2023). Of the 1,089 DECam DDF candidates in COSMOS, 597 (55%) are matched to a DESI spectrum, with 131 of these spectra classified as a galaxy, 432 as a QSO, and 15 as a star. We find some discrepancies between the DESI spectroscopic classifications and Legacy Survey photometric (morphological) classifications for the static-sky counterparts. For example, 41 of the cross-matched DESI galaxies were identified as stars in the Legacy Survey. This simply represents the known challenge of photometric classifications in deep surveys.

To further characterize the DESI and Legacy Survey static-sky counterparts, we present a comparison of the photometric and spectroscopic redshifts in the top panel of Figure 4. Interestingly, it seems that some of our DECam DDF candidates are at higher redshifts ($z > 1.5$) than indicated by the photometric redshifts alone; these will be explored further in future work. There is also one object classified as a star by DESI, but which was classified as a galaxy in the Legacy Survey’s Tractor catalog, albeit with a very low photometric redshift. This object is a bright blue point sources, and most likely a star.

To further characterize the DECam DDF candidates with DESI

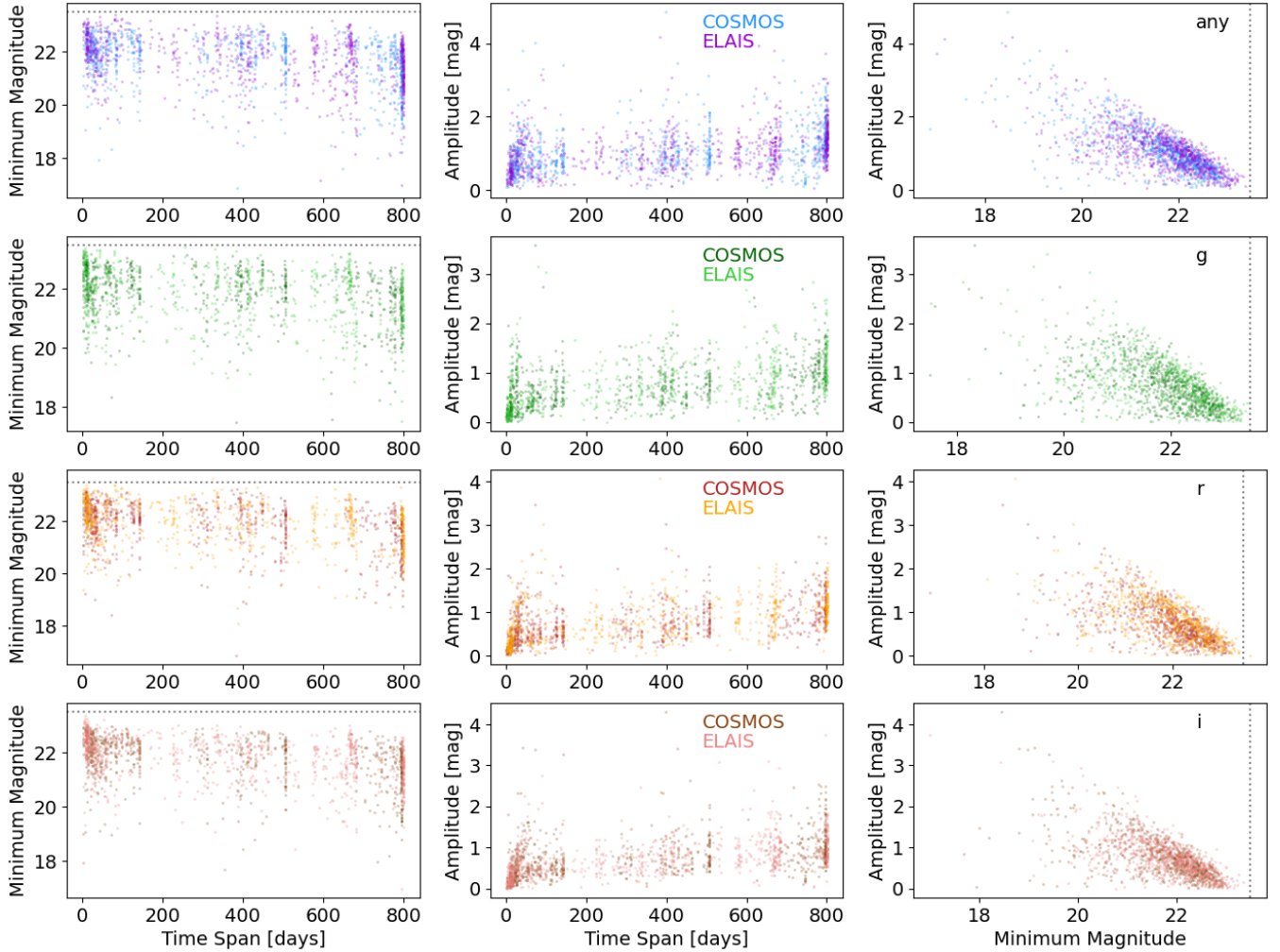


Figure 2. Scatter plots for the nightly-epoch light curve parameters of all 2,020 candidates that passed data-quality cuts.

matches, in the bottom panel of Figure 4 we show scatter plots of the light curve parameters (as in Figure 2) for all candidates in COSMOS with multi-night detections. We can see that the DECam DDF candidates which are matched to DESI galaxies generally have shorter time spans; this makes sense as these candidates are likely transients in host galaxies which were targeted by DESI. On the other hand, DECam DDF candidates which are matched to DESI stars and QSOs have longer time spans and, for the longer-duration events, larger amplitudes and brighter difference-image minimum magnitudes – as expected for variables like stars and QSOs.

Examples of DECam DDF light curves for hosted transients, QSOs (AGN), and variable stars are shown in Section 3. We leave for future work the analysis of the time-domain counterparts of the DESI spectra, and here just comment that all of these data are publicly available.

3 CANDIDATE CHARACTERIZATION

Photometric classification for variable and transient phenomena is a fast-developing field in astronomy, and will be even more essential as future wide-area sky surveys like the LSST which detect millions

of time-domain events – far more than can be followed-up spectroscopically. While we are working towards installing and running published classifiers on the DECam DDF candidates⁷, this paper is focused on simple ways to use the light curve parameters discussed in Section 2.2 to identify and characterize *potential* candidate populations. It is our purpose and hope that this initial analysis will inspire others to take and use the candidate light curves, which are publicly available (Section 2.1).

3.1 Potential Stellar Variables

As mentioned in Section 2, the light curves produced by the processing pipelines and used for this work only include epochs in which the candidate had a *positive* difference-image flux. This precludes most typical analyses of variable stars, such as periodograms. Instead, for this work we provide a preliminary characterization of variable stars in the extragalactic DECam DDFs.

Periodic variables would appear in our data set as candidates with a long time span, but with detections in only a fraction of the epochs

⁷ E.g., the ParSNIP classifier as presented in Boone (2021).

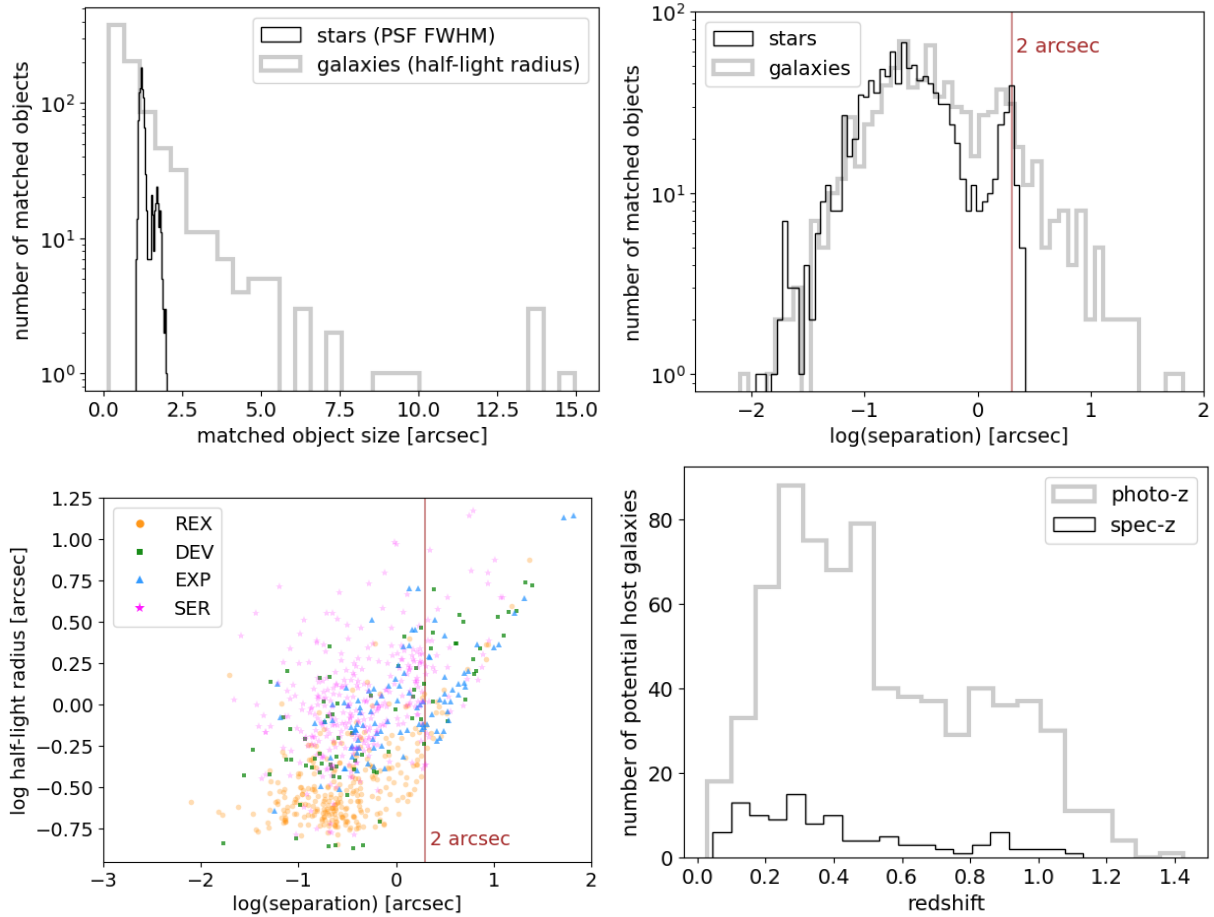


Figure 3. Plots that characterize the Legacy Survey DR10 objects cross-matched to the DECam DDF candidates. The two upper panels include both matched stars and galaxies, while the two bottom panels represent matched galaxies only. At upper left, histograms of the matched object sizes, the PSF full-width at half-maximum (FWHM) for stars and the half-light radius for galaxies. At upper right, histograms of the separation distance between candidate and DR10 object, with an excess at $2''$ which is also the maximum image PSF size. At lower left, the half-light radius versus the separation for galaxies, with point symbol and color based on the best-fit extended-source model. At lower right, histograms of the photometric and spectroscopic redshifts from DR9 for galaxies.

(i.e., when the star is brighter than it is in the reference image). Periodic variables would exhibit a difference-image light curve of alternating detections and non-detections on a timescale of days for short-period variables but weeks to months for longer-period variables. Aperiodic variables that are always brighter in the DECam DDF images than in the reference image might be detected in every epoch, and have varying or similar difference-image magnitudes over the years.

In Figure 5 we show example difference-image r -band light curves for three of the 1081 candidates which were matched to stars in the Legacy Survey (Section 2.4). To identify these three representative examples, we visually reviewed the 34 which exhibited r -band light curve time spans ≥ 750 days, amplitudes ≥ 0.5 mag, minimum magnitudes ≤ 22 mag, and detected in ≥ 70 epochs. In the top panel, DC22icqit appears and disappears as a positive flux source in the difference images on a timescale of days, and could be a short-period variable. In the middle panel, DC21kpm appears to have a slowly varying positive difference-image flux over the 2022A and 2022B semesters (MJD ~ 59750 to ~ 59950). However, it was not detected during the 2021B semester (MJD ~ 59480 to ~ 59600), presumably due to it being fainter than in the reference image. In the bottom panel we show DC21fco as an example of a potential aperiodic variable

star which was always brighter in the DECam DDF images than in the reference image.

3.2 Potential Active Galactic Nuclei

Active Galactic Nuclei (AGN) are known to be variable sources. Optical variability can be used to identify AGN, as well as estimating the mass of the central black hole and accretion disk sizes through techniques like reverberation mapping (see Cackett et al. 2021, for a review of reverberation mapping). Variability in the inner disk propagates outwards, with the same variability observed at longer wavelengths at a later time. This makes large scale photometric surveys useful to study the structure of accretion disks for a large number of AGN.

As mentioned in Section 2 and discussed with respect to variable stars above, the light curves produced by the processing pipelines and used for this work only include epochs in which the candidate had a *positive* difference-image flux. While this precludes a physical analysis of AGN, it is still possible to make a preliminary characterization of potential AGN candidates in the extragalactic DECam DDFs for demonstration purposes. Zhuang et al. (2024) present AGN analysis from their High-quality Extragalactic Legacy-field Monitoring

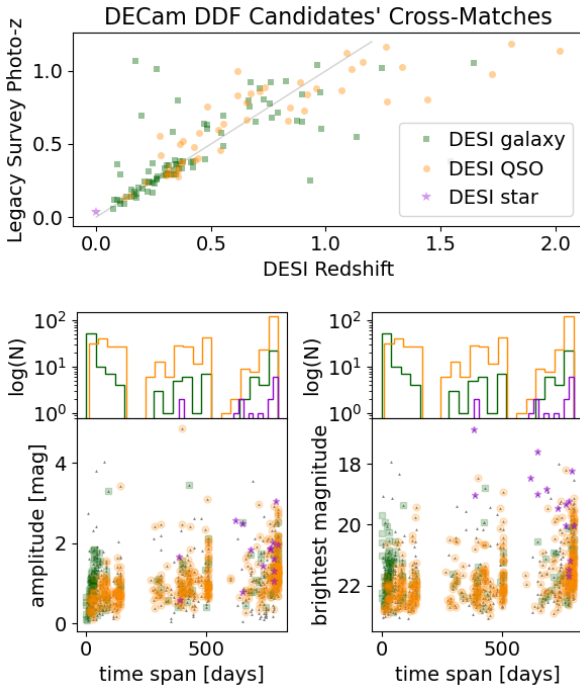


Figure 4. Top: the Legacy Survey photometric redshifts versus the DESI redshifts for static-sky objects cross-matched to the DECam DDF candidates. Symbols and point color represent the DESI classifications as in the legend. Bottom: scatter plots of the DECam DDF light curve parameters for all candidates in COSMOS with multi-night detections (small triangles), and for candidates cross-matched to DESI objects. Histograms demonstrate how the time span distributions for galaxies (green) and QSO (orange) are similar.

(HELM) program, which includes COSMOS and ELAIS DECam DDF images.

3.2.1 Cross-matches to AGN in SIMBAD catalogs

As the COSMOS and ELAIS deep drilling fields are legacy fields with a long history of astronomical observations, many of the AGN have already been detected through various techniques (e.g., spectroscopy, photometric variability), in different wavelengths (e.g., X-rays). As presented in Rollins et al. (2023), we retrieve a heterogeneous sample of AGN in COSMOS or ELAIS from a variety of catalogs available via SIMBAD (Wenger et al. 2000): the COSMOS2015 galaxies catalog (Laigle et al. 2016), the Advanced Camera for Surveys General Catalog (SCSGC; Griffith et al. 2012), the ESO Spitzer Imaging extragalactic survey (ESIS; Berta et al. 2006), and the Spitzer Wide-Area Infrared Extragalactic Survey (SWIRE; Lacy et al. 2013).

We find that 466 of the 2,020 candidates are matched to an already-known AGN. Most are classified as quasi-stellar objects (QSOs; 325) or AGN (119), and a few are Seyfert galaxies (20). The catalog we retrieved from SIMBAD is both very heterogeneous and contains many duplicate sources, and we consider it beyond the scope of this work to draw inferences about, e.g., the fraction of AGN which were identified by spectroscopy or X-rays emission that are optically variable (or vice versa).

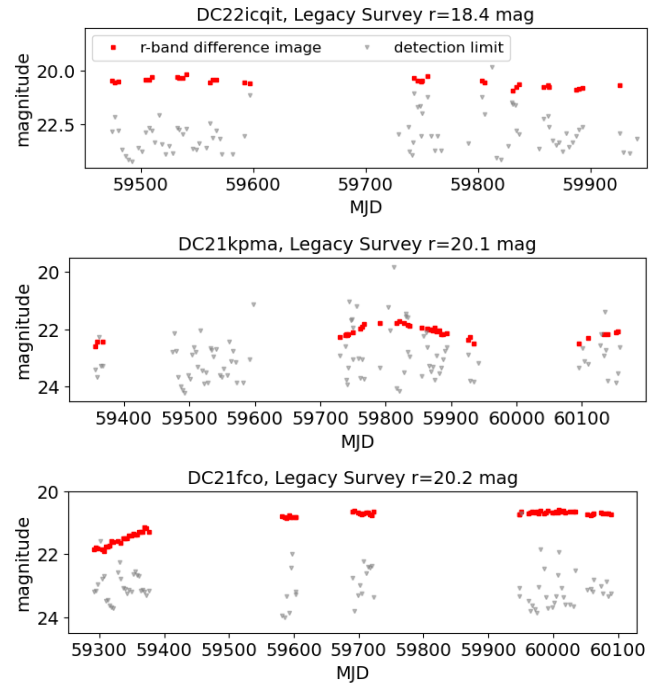


Figure 5. The r -band difference-image light curves (for positive difference-image flux detections only; red squares) for a few selected potential stellar variables in the DECam DDF extragalactic fields. Small grey symbols represent the r -band nightly-epoch limiting magnitude estimates.

3.2.2 Potential AGN light curves

Variability in AGN can be described as stochastic, and has typical timescales of months and years, with average variability in the order of 10-20% (Vanden Berk et al. 2004). To find candidates that are potential AGN, we apply constraints on the nightly-epoch light curves based on general characteristics of AGN variability. We expect they would show up for the duration of the survey, disappearing for periods where the field is not visible, or when the AGN brightness is fainter or not significantly different than the template. Therefore we set a minimum time span of two years, a minimum difference-image magnitude of 23 mag, a minimum amplitude of 0.2 mag, and a minimum number of 40 epochs in any filter (g , r , or i). Since AGN emission is nuclear, we add the constraint that if the candidate is matched with a galaxy based on the Tractor catalog, then it should also be in the core of the galaxy. There are 254 candidates that meet the restrictions on their photometric variability from the DECam DDF, and 131 are cross-matched to already-known AGN. Adding the restriction that these conditions be met on all three filters reduces the number of candidates to 54 and 28 respectively.

To demonstrate what potential AGN light curves look like in the DECam DDF's difference-image photometry, Figure 6 shows the light curves of three candidates that display stochastic, long term variability in any of the g , r , i bands, and are matched to a galaxy core. In the top panel, DC21by is a known QSO in the COSMOS field. Gaps in the data points are partly due to observing gaps (roughly corresponding to semesters 2021B and 2022B), and partly due to the candidate being fainter or of similar brightness to the template image. Two additional light curves were chosen to show in Figure 6 due to their similarity with known QSO DC21by. In the middle panel, DC23kgtj shows a similar light curve to DC21by, but is not matched to a known AGN. It is briefly not detected in the i -band around MJD

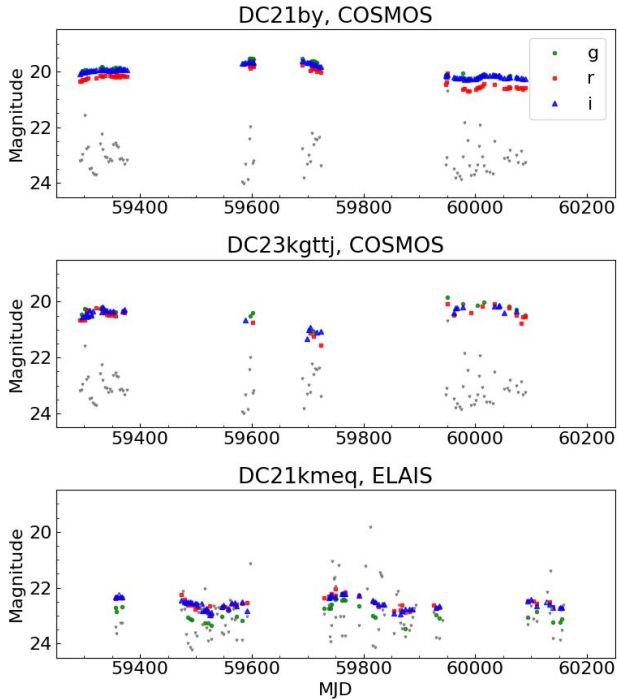


Figure 6. Difference image g, r, i photometry vs modified Julian Date (MJD) light curves for three candidates. DC21by is a known QSO, and DC23kgttj and DC21kmeq are examples of potential AGN in the COSMOS and ELAIS DDF. Small grey symbols represent the r -band nightly-epoch limiting magnitude estimates.

60000, when it probably had a brightness similar to or fainter than the template image. In the bottom panel, DC21kmeq is another example of a potential AGN that was not matched to a known AGN in the ELAIS field. Gaps in the data points roughly coincide with semesters 2021A, 2022A and 2023A. Around MJD 59800, it is possible it was too faint for detection. In Figure 7, we show color images from the Legacy Survey DR9 at the location of these three candidates, all of which are point-like and suggest that DC21kmeq and DC23kgttj are QSO like DC21by.

In our visual review of the potentially AGN-like candidates that were cross-matched to the center of their potential host, the light curve of DC21kslv stood out as different from the potential AGN shown in Figure 6. The light curve of DC21kslv, shown in Figure 8, exhibits a smooth rise over ~ 70 days, with the peak occurring at a magnitude of 20.06 (in the g -band), around MJD ~ 59520 , and then slowly declines – at first glance, appearing almost transient-like. However, the duration of the rise is longer than for supernovae and longer than seen for tidal disruption events (TDE) like, e.g., PS1-10jh (Gezari et al. 2012). Although at first glance DC21kslv looks special, given its early detections around MJD 59350 days, its late time rise at 60100 days, and its stellar-like appearance in Figure 7, we suspect it is probably just a QSO.

The takeaway message from this preliminary analysis is that the DECAM DDF does provide rich time-domain information for AGN for future analyses, but that the applications of difference-image photometry alone for AGN are limited.

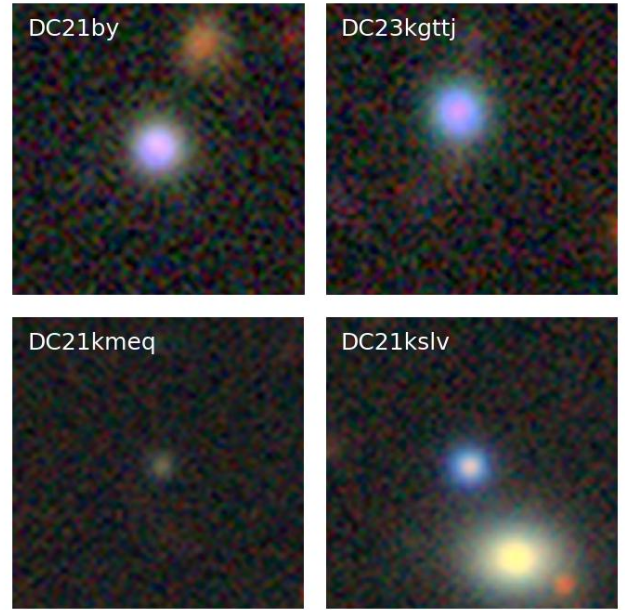


Figure 7. Color images from the Legacy Survey DR9 at the location of four candidates selected for their AGN-like variability with light curves shown in Figures 6 and 8.

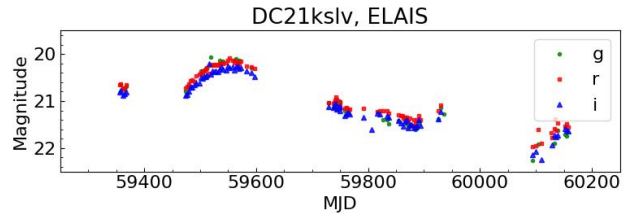


Figure 8. Difference image g, r, i -band photometry versus modified Julian Date (MJD) lightcurves for variable nuclear candidate DC21kslv.

3.3 Potential Type IIP Supernovae (SN IIP)

Type II supernovae (SN II) are caused by the core collapse of massive stars. SN IIP light curves are heterogeneous in their peak brightness, but typically exhibit a ~ 100 -day "plateau" phase of slow decline after peak brightness (Arcavi et al. 2012), which is unique among supernova types. This plateau occurs when the hydrogen envelope surrounding the progenitor star is retained before core collapse (Smartt et al. 2004). In our original proposal for the DECAM DDF, we had estimated finding ~ 5 SN IIP per semester based on volumetric explosion rates (i.e., with no loss due detection or classification efficiencies).

To find potential SN IIP among our candidates, we first identify 243 candidates with r -band light curve time spans between 50 and 150 days. We calculate the r -band light curve slope in magnitudes per day for observations between 15 and 80 days after the first detection. This would be the "plateau" phase for any candidates that are SN IIP. We then restrict to only those candidates with slopes of less than 0.03 magnitudes per day, over at least 40 days, and with at least 7 epochs (nights detected). This is still a very generous range of parameter space, as a full SN IIP light curve would decline by < 3 magnitudes

Name	Peak m_r	Tractor Catalog Match			
		Type	m_r	z_{phot}	M_r
DC21daldo	21.93	SER	22.38	0.37 ± 0.15	-19.6
DC21jay	21.62	EXP	22.31	0.29 ± 0.38	-19.3
DC22hxfqh	21.39	SER	20.18	0.12 ± 0.06	-17.3
DC22iykhs	21.98	EXP	21.94	0.48 ± 0.11	-20.2
DC23jmrjg	21.57	SER	21.12	0.25 ± 0.08	-18.9
DC23jmszp	21.97	PSF	22.88	N/A	N/A
DC23kzuyh	20.41	REX	21.04	0.47 ± 0.04	-21.7

Table 1. For the seven candidates identified as potential SN IIP based on their light curves, the peak r -band magnitude is shown in column 2. Characterization parameters for the matched object from the Tractor catalogs in column 3 to 5 are the best-fit model type, the static-sky r -band magnitude and the photometric redshift (as described in Section 2.4). In column 6 we show the estimated peak absolute brightness for the candidate based on the photometric redshift, assuming a flat cosmology.

over 100 days and, with the DDF’s cadence, likely be detected on >7 nights.

These simple, generous restrictions result in 42 candidates with a slow decline over at least a few weeks post-peak for visual review. Of the 42, most appear to be active galactic nuclei in that their light curves rise and decline non-monotonically, but 7 do meet the description of a potential SN IIP in their time span and slow decline. The light curves for these seven are shown in Figure 9, along with one additional candidate of interest which was identified from among the 42 as a potential tidal disruption event (Section 3.4). In this set, DC22hxfqh is an oddity with a long-duration rise in the i -band over a ~ 90 -day “plateau” phase.

The utility of a deep-drilling style program is evident from the shorter-timescale features that are on display in the light curves in Figure 9. For example, DC21daldo, DC21jay and DC23jmszp exhibit light curve “bumps” that are reminiscent of Type II_n supernovae, in which the ejecta material interacts with circumstellar material and can cause re-brightenings as was seen for, for example, SN 2009ip (e.g., Mauerhan et al. 2013; Pastorello et al. 2013; Graham et al. 2014). We note that although the “bump” in the light curve for DC23jmszp at around 40 days past peak is a similar timescale to the first bump in the light curve of SN 2009ip, the two events are actually not overall that similar because SN 2009ip declined by ~ 2 magnitudes on that time scale, and DC23jmszp does not (and neither do DC21daldo or DC21jay). Another example of the benefit of the deep-drilling style program is that for most of these seven potential SN IIP, the g -band declines much more rapidly but thanks to the 2–4 cadence of the DECam DDF, is still well-sampled in this dataset.

Finding seven potential SN IIP over five semesters is well off the prediction from the original proposal of ~ 5 per semester, but notice in Figure 9 that our rough restrictions have yielded only the brightest events. These seven all reach peaks brighter than 22 mag, whereas our predicted yields were based on the detection limits of ~ 23.5 mag. Longer duration transients like SN IIP are one of the event types whose detection efficiency with this DDF program would benefit significantly from difference imaging with nightly stacked images, which remains work in progress (Section 4).

3.3.1 Cross-matches to the Tractor catalog

Of the seven candidates identified, all of them are matched to an object in the Tractor catalog, as shown in Table 1. Six of these objects are classified as galaxies, but the object at the location of DC23jmszp

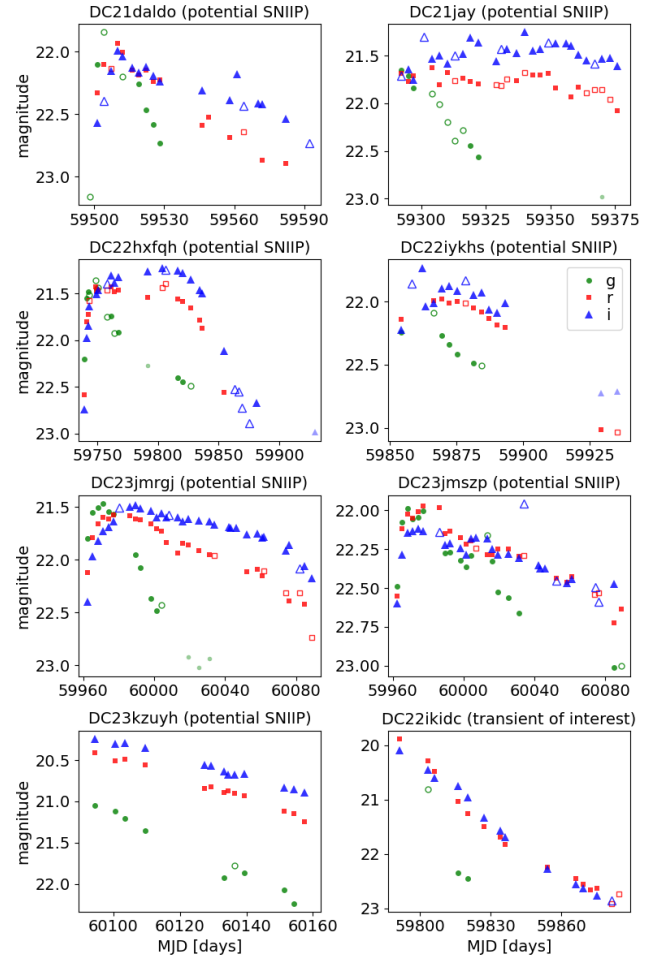


Figure 9. The DECam DDF multi-band light curves for seven potential SN IIP identified with simple restrictions on the light curve parameters, and (at lower right) one transient of interest (DC22ikidc) which also made the initial cuts, but is not SN IIP-like. Open symbols represent a nightly-epoch photometry point with a mean real-bogus score of < 0.4 (closed symbols represent ≥ 0.4 , and transparent closed symbols represent “lonely epochs” as described in Section 2.2).

is classified as a star. Color image stamps for all seven (plus the candidate of interest DC22ikidc) are shown in Figure 10. They generally show the bluer spiral (or irregular) galaxies with ongoing star formation that is typical for the hosts of core-collapse supernovae. For the six candidates matched to galaxies with photometric redshifts (none of the matches have spectroscopic redshifts), the inferred peak r -band absolute magnitudes range from -17 up to almost -22 . For SN II, peak intrinsic brightnesses from -14 to -19 mag can be considered as within the range of expectation (e.g., Li et al. 2011; Anderson et al. 2014; Sanders et al. 2015; Hillier & Dessart 2019). However, for example DC23kzuyh with an estimated peak of -21.7 mag would be more appropriate for a superluminous supernova (SLSN; Quimby et al. 2007; Gal-Yam 2019).

3.4 Candidate DC22ikidc: A Tidal Disruption Event?

As described in Section 3.3, DC22ikidc was identified as a potential SN IIP based on broad cuts to the light curve parameters. However, its light curve stands out from the other SN candidates’ in Figure 9

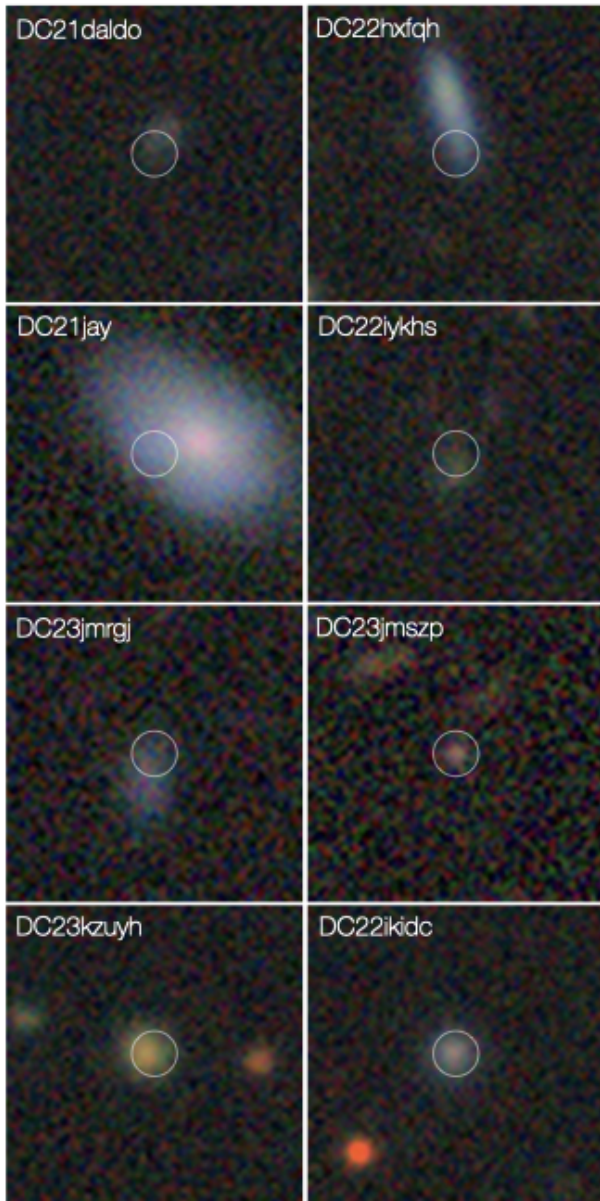


Figure 10. The locations of the eight candidates whose light curves are shown in Figure 9 in the Legacy Survey DR9 color image (oriented north up, east left). These stamps are all $\sim 14'' \times 14''$ and centered on the candidates' coordinates, for which a light circle is drawn to guide the eye.

because its long-term near-linear (in magnitudes) decline is more reminiscent of a tidal disruption event (TDE). In Figure 11 we compare the DECcam DDF's r -band light curve of DC22ikidc to the r -band light curves for two TDEs from the literature with well-sampled declines: ASASSN-14ae (Holoien et al. 2014) and iPTF16axa (Hung et al. 2017). The two comparison light curves have been shifted in date, and ASASSN-14ae has been shifted in magnitude, to align with DC22ikidc. Unfortunately there is no way to constrain the event start date for DC22ikidc, as the nearest epoch with a limiting magnitude was 22 days before detection (it was $r \sim 23.7$ mag).

Although DC22ikidc does decline more rapidly than the two TDEs shown in Figure 11, considerable diversity is emerging among TDEs (e.g., van Velzen et al. 2020; Charalampopoulos et al. 2023). Without spectra or observations across the electromagnetic spectrum it will

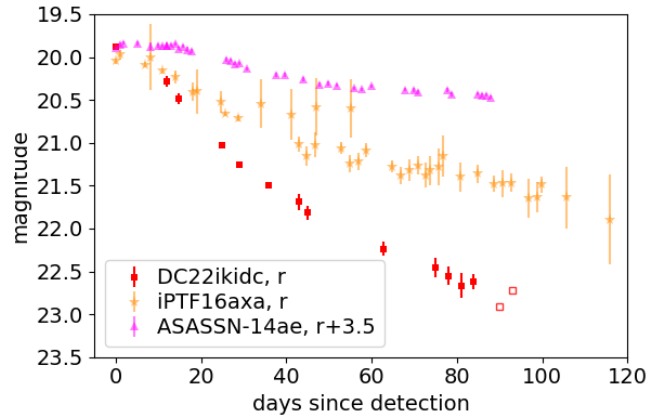


Figure 11. The DECcam DDF r -band light curve of candidate DC22ikidc (red squares) compared to the r -band light curves for TDEs ASASSN-14ae (pink triangles) and iPTF16axa (orange stars).

be hard to confirm the true nature of DC22ikidc. However, it was located right in the core of its host galaxy, as shown in the lower-right panel of Figure 10. In the Tractor catalog, the host galaxy has a type of REX, an apparent r -band magnitude of 21.35 mag, and a photometric redshift of 0.22 ± 0.10 . This photometric redshift gives DC22ikidc an intrinsic magnitude of about -20 ± 1 mag (the error is based on the estimated error in the photometric redshift), which is typical for TDEs (e.g., van Velzen et al. 2020).

3.5 Potential Type Ia Supernovae (SN Ia)

In our original proposal for the DECcam DDF, we had estimated finding (per semester) ~ 20 SN Ia within a redshift of $z < 0.5$, and one to two $z < 0.25$ SN Ia within four days of explosion. Although these estimates were for the originally-proposed 2-day cadence, did not include detection or classification efficiencies, and were for anticipated processing that used deeper nightly image stacks for the difference-image detections (which is still in development), they are still in the ballpark for what we might expect from the implemented DECcam DDF survey. As we did not have a program to spectroscopically follow-up DECcam DDF targets, and we are leaving photometric classification (using software based on e.g., machine learning or template-fitting) to future work, we instead develop an informal process to identify *potential* SN Ia among the candidates.

Since SN Ia light curves are homogenous, events at lower redshifts reach brighter apparent magnitudes and are detectable for longer (in surveys with a constant limiting magnitude, like the DECcam DDF). Using template light curves from Nugent et al. (2002) we derive an approximate linear relationship (for the DDF's limiting magnitudes) between light curve amplitude A and time span D for filter f , such that SN Ia have $A_f > m_f D_f + b_f$ where the slope values are $m_g = 0.050$ and $m_r = m_i = 0.037$ mag per day and the intercepts are $b_g = b_i = -1.5$ and $b_r = -1.125$ mag. Light curve amplitude and time span are two of the light curve parameters we had already calculated for all candidates (Section 2.2), so these approximate relations allow us to use these parameters to identify potential SN Ia. We take as potential SN Ia all candidates which meet the following conditions in at least two of the three filters: light curve time span is ≥ 10 and ≤ 200 days; amplitude ≥ 0.5 mag; number of nights detected ≥ 5 ; and $A_f > m_f D_f + b_f$ for filter f . This yields 100 potential SN Ia out of all our DECcam DDF candidates.

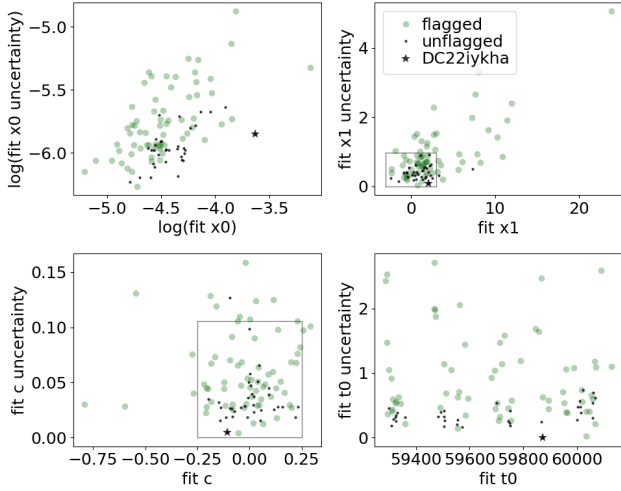


Figure 12. The `sncosmo` best-fit SALT2 model light curve parameters of x_0 (related to peak brightness), x_1 (related to light curve decline rate), c (related to color at peak brightness), and t_0 (time of peak brightness), for the 66 flagged (green circles) and 34 unflagged (black dots) potential SN Ia candidate light curves. The black star is the special case of candidate DC22iykha. Grey boxes represent the typical ranges of the x_1 and c parameters for SN Ia (x -axis limits) and the uncertainties for unflagged light curves (y -axis limits). There are 62 candidates with parameters in both boxes; 31 each of flagged and unflagged candidates.

To all 100 potential SN Ia we apply the `sncosmo` light curve fitting code (Barbary et al. 2023). We chose `sncosmo` because it is python-based and works off-the-shelf with optical light curves. With `sncosmo` we use the SALT2 model (Guy et al. 2007). The idea was to use `sncosmo` to fit the light curves as if they were SN Ia, and then use the fit parameters to make a probabilistic assessment of a candidates’ likelihood of being a SN Ia. Before running `sncosmo` we visually review the light curves of all 90 potential SN Ia candidates and flag those which are not well-sampled enough to expect a decent light curve fit with `sncosmo`. Candidates are flagged if their light curve is missing a filter, missing the rise or the decline in all three filters, the decline is sampled with <3 epochs or ≤ 15 days in two or more filters, or if the light curve does not approximately monotonically rise and fall like a transient (i.e., if it fluctuates more like an AGN). Of the 100 potential SN Ia, 34 have unflagged light curves.

As an input to `sncosmo` we estimate the redshift of the candidate by assuming that it is a SN Ia, that its brightest observed magnitude is its peak magnitude, and that the intrinsic peak brightness of SN Ia is -19.3 magnitudes. We then pass upper and lower boundaries on redshift of ± 0.15 from this estimate to `sncosmo`. If the lower boundary is < 0.05 , which is the lower limit of `sncosmo`, then boundaries of 0.05 to 0.35 are passed instead (i.e., the same range width). We acknowledge that starting off with an assumption that the candidate is a SN Ia, and passing a redshift based on that assumption, means that `sncosmo` is more likely to fit a SN Ia light curve, even if the event was another type of supernova.

In Figure 12 we show scatter plots of the SALT2 light curve parameters fit by `sncosmo` for the 66 flagged and 34 unflagged potential SN Ia candidates. These SALT2 parameters are x_0 (related to peak brightness), x_1 (related to light curve decline rate), c (related to color at peak brightness), and t_0 (time of peak brightness). From these plots we can see that the idea to use the fit values and uncertainties to assess whether a candidate was a SN Ia was a bit naive. As shown

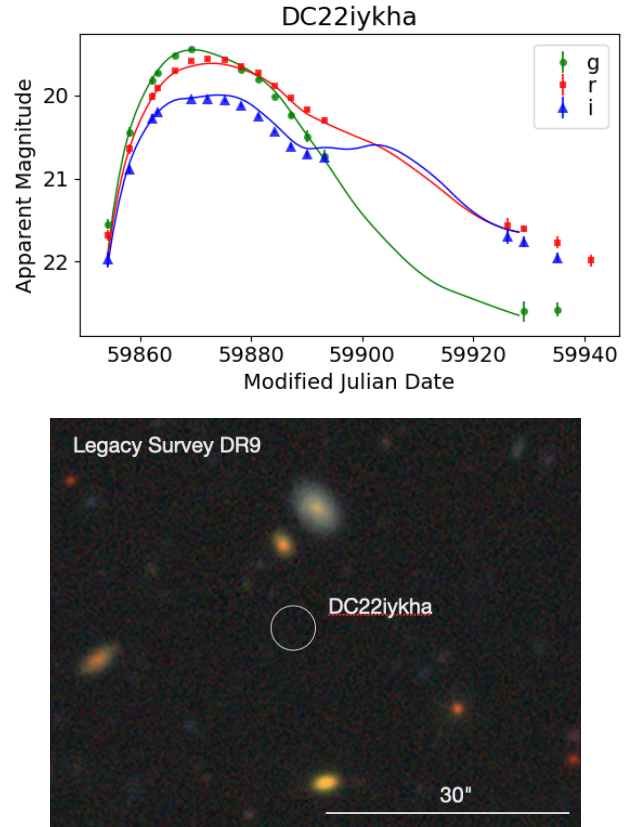


Figure 13. Top: The DECam DDF multi-band light curve of candidate DC22iykha (points), and the best fit SALT2 model SN Ia light curve by `sncosmo` (lines). Bottom: The location of candidate DC22iykha in the Legacy Survey DR9 color image (oriented north up, east left) reveals it to be potentially hostless.

in Figure 12, the flagged candidates (green circles) do have higher uncertainties and a broader ranges of fit parameters returned. In some cases these are beyond the ranges for true SN Ia, which are marked by the boxes in the upper-right and lower-left panels: $-3 < x_1 < 3$ and $-0.25 < c < 0.25$ (Hicken et al. 2009; Garnavich et al. 2023). However, in general there is significant overlap between the unflagged and flagged candidates. In other words, even a poorly-sampled candidate light curve can still return SN Ia-like fit parameters. In total, there are 62 candidates in the boxes in the x_1 and c panels of Figure 12, 31 each of flagged and unflagged candidates.

The main takeaway of this analysis is that overall, the DECam DDF caught 62 candidates in 2 years that are decently fit as a SN Ia using the SALT2 model and `sncosmo`. The original estimate of ~ 20 per semester (~ 100 over five semesters) was off by about a factor of 2. This is not surprising, given that this work is using detections in single images instead of nightly coadds, and that the cadence was lower than initially anticipated. The good news, however, is that if proper photometric classification is applied to this now-public data set, SN Ia science relating to rates or host galaxies should be possible. All are welcome to use this list of 100 potential SN Ia as a starting point for further work.

3.5.1 Candidate DC22iykha

One particular candidate of interest, DC22iykha, is a bright outlier among the potential SN Ia, and is marked with a black star symbol

in Figure 12. DC22iykha has a bright high-fidelity light curve, as shown in the top panel of Figure 13. Although at first glance the *sncosmo* fit does seem appropriate, the error bars on the photometry are small and the systematic offset in the *r*- and *i*-bands is significant. Although the *i*-band does give a hint of the onset of the *i*-band bump that is common in SN Ia light curves, the apparent $r - i$ color is bluer than a typical SN Ia (which is closer to 0). We checked if the host galaxy or environment held any additional information for this candidate by reviewing the Legacy Survey DR9 color cutout⁸ shown in the bottom panel of Figure 13, and found that this candidate is potentially hostless. The cross-matching with the Tractor catalog described in Section 2.4 finds this candidate to be offset by $1.7''$ from a galaxy that has a photometric redshift of 1.07 (but an uncertainty of 0.59), which is not visible in the color image shown in Figure 13. If it exists, it is more likely a background galaxy that is unassociated with candidate DC22iykha. A cross-match with the Transient Name Server⁹ reveals that this event was discovered and reported by the Asteroid Terrestrial-impact Last Alert System (ATLAS; Tonry et al. 2018) on 2022-10-20 and was assigned the designation AT 2022yfq (Tonry et al. 2022).

3.5.2 Cross-matches to the Tractor catalog

Of the 100 candidates identified as potential SN Ia, only three are not matched to a Tractor catalog object, and for 84 the best match is a galaxy. For the remaining 13 the best match is a star, but for ten of these there is also a galaxy that is near enough to be considered a potential host. Considering only the 34 unflagged candidate light curves of potential SN Ia, only one is not matched (DC23jsner; but see Section 3.8) and 29 are matched to a galaxy. Four are matched to a star, but for three there is also a galaxy near enough to be considered a potential host; one is another potentially hostless transient (DC21jfc). This work has not used any information about potential host galaxies (or stellar counterparts) to identify potential SN Ia, nor used the potential host photometric redshifts as a prior in any of the *sncosmo* fits. However, we mention the cross-matches here to illustrate the fact that there is likely useful potential-host information that could and should be incorporated into future photometric classification efforts and SN Ia analyses.

3.5.3 Potential SN Ia Caught Early

One of the science goals of the DECam DDF was to find transients, and in particular SN Ia, within a few days of explosion. In our original proposal, we estimated that the DECam DDF could catch ~ 1 SN Ia at $z \lesssim 0.25$ within four days of explosion per semester, but again this was based on the originally proposed two-day cadence. Multi-band photometry of SN Ia at early stages can exhibit signatures of the binary companion star, of circumstellar material, and/or of the mixing of radioactive material into the outer layers of the exploding white dwarf star (as discussed in, e.g., Kasen 2010; Piro & Morozova 2016; Hosseinzadeh et al. 2017; Dimitriadis et al. 2019). In this work we make a preliminary investigation of how many potential SN Ia were detected at early times, whether any obvious deviation from a template light curve is evident.

SN Ia light curves are known to have rise times (the time between explosion and peak brightness) of around 19 days, plus or minus a few days (Riess et al. 1999; Firth et al. 2015). Cosmological time

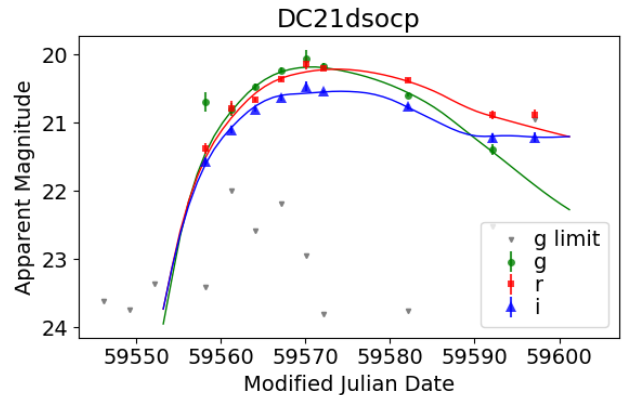


Figure 14. The DECam DDF multi-band light curve of candidate DC21dsocp (points), and the best fit SALT2 model SN Ia light curve by *sncosmo* (lines). Grey inverted triangles represent the *g*-band nightly-epoch limiting magnitude estimates.

dilation will also increase the rise times by a few days at $z = 0.2$ (i.e., by a factor of $1 + z$). Of the 34 unflagged potential SN Ia identified, we find that 17 were first detected between 14 and 28 days before the date of best-fit peak brightness from *sncosmo*. Of the 17, four have a fit redshift and peak brightness that suggest they are $z \lesssim 0.25$ events, which does approximately match with the ~ 1 per semester that was originally predicted. One of these four, DC21dsocp, exhibits a potential deviation from its best-fit template light curve in its earliest *g*-band detection, as shown in Figure 14. This potential deviation is later in time, as in closer to peak brightness, than for SN Ia for which early-time deviations have been previously detected (e.g., Hosseinzadeh et al. 2017; Dimitriadis et al. 2019). Without spectroscopy or a fuller light curve, it is unclear even whether DC21dsocp is a SN Ia; perhaps the *g*-band excess is a shock breakout or other phenomenon for a core collapse SN. It is beyond the scope of this work to say any more than such photometric anomalies are detectable in this data set.

The DECam DDF observation blocks were designed such that, during a DECAT night, they did not need to be done consecutively (i.e., all observations obtained within an hour). Having the option to spread the DDF blocks out was intended to both help with scheduling multiple programs and to potentially make the intra-night photometry more useful by raising the potential of detecting intra-night rising or declining events. However, in practice, all DDF blocks were usually obtained within an hour. Of the 17 candidates detected > 14 days before peak, only five had two or more detections in the individual difference images in at least two bands in their first night of detection. In all cases these detections were all obtained within an hour of each other and no intra-night rise is discernable (as might be detectable if they happened to be caught within hours of explosion).

3.6 Potential Fast Transients

Fast transients are short time-scale transients whose brightness rises and falls within days to weeks. Types of fast transients include fast blue optical transients (Drout et al. 2014), and the optical counterparts of short gamma-ray bursts gravitational wave events such as kilonovae (KN). In the original proposal for the DECam DDF, we estimated finding up to 1 rapidly evolving transient per semester.

To identify potential fast transients among the DECam DDF candidates, we first identify candidates with a light curve time span

⁸ <https://www.legacysurvey.org/>

⁹ <https://www.wis-tns.org/>

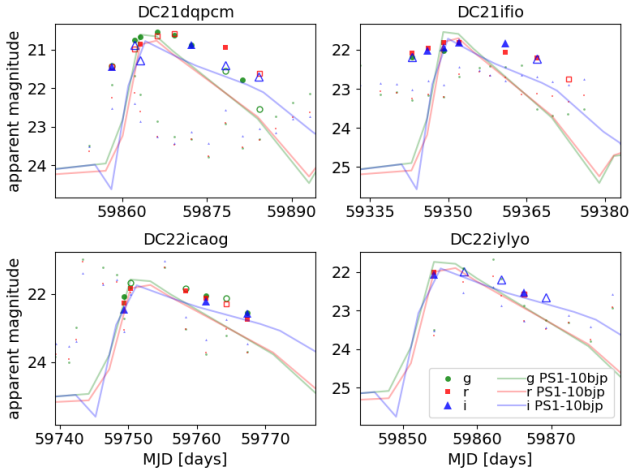


Figure 15. The DECam DDF multi-band light curves for four candidates identified with light curve parameter cuts as potential fast transients. Large symbols have the same meaning as in Figure 9 and small symbols represent the r -band nightly-epoch limiting magnitude estimates. The solid lines represent the photometry of PS1-10bjp from Drout et al. (2014), shifted to approximately match in the r -band.

parameter less than 30 days in *every* filter, and which in at least one filter was detected at least three nights; reached a peak brightness ≤ 22 mag; had an amplitude parameter of ≥ 0.5 mag; and had a rise time of ≤ 10 days. This results in 21 candidates for visual review. After rejecting candidates that have multiple peaks, a slow decline, or only a rise, we are left with four candidates. None of the 21 potential fast transients we have identified declined as quickly as the KN associated with gravitational wave event GW170817, which declined by about 4 magnitudes in 10 days in g - and i -band (Cowperthwaite et al. 2017). The three-day cadence of the DECam DDF is a bit too long to confidently identify KN.

In Figure 15 we show the DECam DDF light curves for these four candidates, along with the light curves of fast transient PS1-10bjp from Drout et al. (2014) for comparison. PS1-10bjp was chosen for being the best observed object of the sample, and it has been shifted to approximately match each DDF candidate in the r -band. We can see that the two candidates in the top panels of Figure 15, DC21dqpcm and DC21ifio, are probably not fast transients after all, as they rise and decline more slowly than PS1-10bjp. While the candidates in the two lower panels, DC22icaog and DC22iylyo, appear to match PS1-10bjp fairly well, DC22icaog lacks detection limits to confirm the fast decline and DC22iylyo lacks pre-detection limits to confirm a fast rise.

We additionally check the individual difference-image photometry from the first night that DC22icaog was detected, in case the DDF blocks were spread out sufficiently to identify an intra-night rise. As was the case for SN Ia (as described at the end of Section 3.5.3) no intra-night evolution in the magnitude of DC22icaog was detectable.

All four of these candidates are cross-matched to galaxies in the Tractor catalog, as shown in Figure 16. These galaxies have photometric redshifts which, under the assumption of a flat cosmology, result in estimated peak absolute magnitudes in the r -band of -19.19 mag for DC21dqpcm, -19.43 mag for DC21ifio, -18.67 mag for DC22icaog, and -20.19 mag for DC22iylyo. These estimates are consistent with the range of -16.5 to -20.0 mag for fast transients from Drout et al. (2014). However, given the poor constraints before

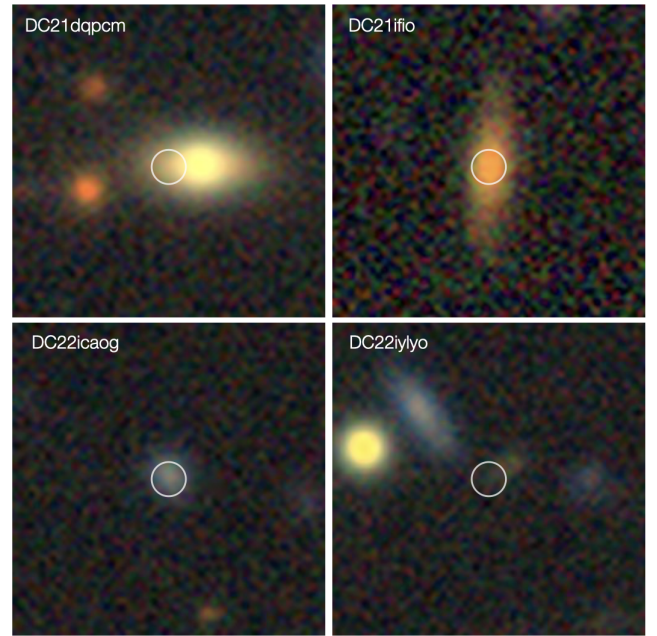


Figure 16. The locations of the four candidates whose light curves are shown in Figure 15 in the Legacy Survey DR9 color image, in the same manner as Figure 10.

the first (and after the last) detections for each of these candidates, ultimately none can be confirmed as potential fast transients.

3.7 Potential Lensed or Superluminous Supernovae

We search the sample for potential rare and bright objects like strongly gravitationally lensed supernovae. Due to magnification from lensing, they are expected to be brighter than the nominal absolute magnitude for their transient class at the source redshift. For objects like Type Ia supernovae, which have a small dispersion in their peak brightness, this is a powerful method to discover such object (Goldstein & Nugent 2017). We note that based on previous predictions (e.g., Goldstein et al. 2019a) we also expect to find many lensed core collapse SNe (CCSNe), however, since their peak luminosity has a large intrinsic dispersion, we require a different selection method to identify them in the data. Therefore, for this analysis, we only focus on the lensed SNe Ia, but will expand the search to include all types of lensed SNe in future work. The method based on the magnification has been used in the real-time discovery of the two galaxy scale lensed Type Ia supernovae discovered in wide field surveys, namely iPTF16geu Goobar et al. (2017) and SN Zwicky (Goobar et al. 2023). Within this search method, we start with the subsample that has a spectroscopic redshift, so that the distance modulus to the source – and hence the absolute magnitude – can be accurately measured. We also analyse the subsample of objects that have a photometric redshift with an accuracy better than $\sigma(z) = 0.02$ corresponding to a distance modulus error < 0.1 mag at typical redshifts $\sim 0.5 - 1$ where we expect the SNe to be observed (Arendse et al. 2023).

From the first method, when using a spectroscopic redshift of the galaxy associated to the transient we find 109 objects with an existing redshift. We also make the quality cuts applied above for potential SNe, i.e. > 5 nights where the transient was detection and a duration

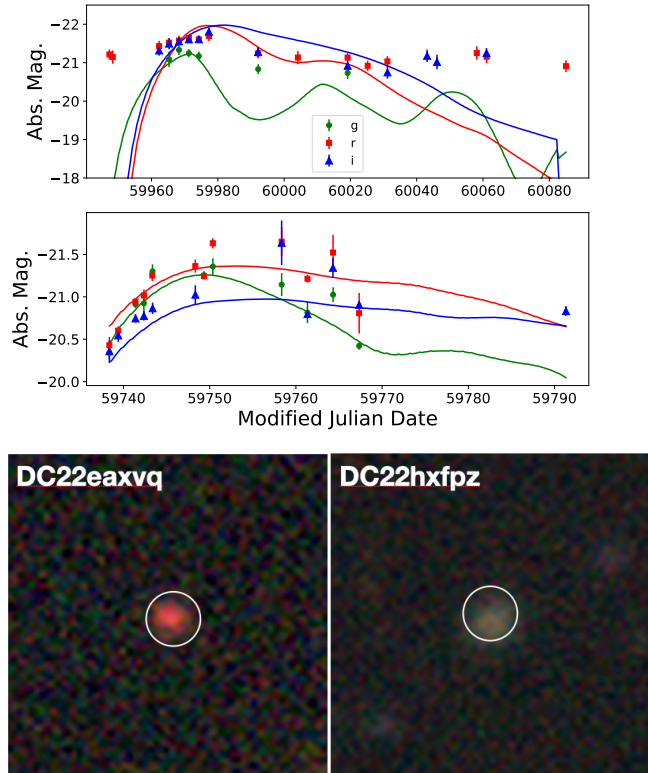


Figure 17. Two most likely lensed SN candidates - DC22eaxvq (top) and DC22hxfpz (middle) - based on their peak brightness from the distance modulus inferred using the photometric redshift as well as visually inspecting the lightcurve to verify SN-like evolution (i.e. an inflection point a few weeks from the first observation). The solid lines are the fits to the doubly imaged SN Ia model, showing no strong evidence that these candidates are lensed SNe Ia. At bottom, the Legacy Survey DR9 color images at the locations of the two candidates.

> 10 d and < 200 d. The latter cut is made to remove objects that are intrinsically bright and long-lived and may have peak luminosities similar to lensed SNe Ia, e.g. AGNs and TDEs. We also make the absolute magnitude cut of $M_g < -20$ mag as defined in (Goldstein & Nugent 2017) which leaves us with 2 candidates: DC21cwsvw and DC23ldice. DES21cwsvw has only a few points in the g and r filters, making any further inference difficult. Fitting the lightcurve of DC23ldice, we find that the SN Ia template fit suggests very blue colours which is not expected for lensed SNe Ia based on the observations of recent lensed SNe Ia (Goobar et al. 2017, 2023), for which the $g - r$ colours at peak are > 0 mag.

We analyse the sample with small photo- z errors using the same criteria as the spec- z sample. From visual inspection we find two candidates: DC22eaxvq and DC22hxfpz that have SN-like lightcurves showing both a sharp rise to and decline from peak (Figure 17). DC22eaxvq shows an inflection in the r and i filters and has a peak $g - r$ colour of 0.26 mag. One sign that a transient could be a lensed SN is that the SALT2 lightcurve shape parameter $-x_1$ is wider than the typical value of cosmological SNe Ia, i.e. $-3 < x_1 < 3$ ($x_1 = 5.95 \pm 0.93$), which could be due to the superposition of more than one SN image or because the true redshift is higher than the associated redshift. From a SALT2 model fit to DC22eaxvq, we infer a large x_1 which could suggest that the lightcurve is a summation of

more than one image with a time-delay. Given this lightcurve shape and bright peak luminosity, we test whether a multiply imaged SN Ia model would fit the data better than a single point. We use sntd (Pierel & Rodney 2019) to fit a doubly imaged SN Ia to the data (solid lines in Figure 17). While the doubly imaged SN Ia model fits better than the single SN Ia model, the fit only converges for fixed magnifications ratios. The reduced χ^2 of the fit is > 10 suggesting that the multiply imaged SN model does not explain the data. A spectrum while the transient was live would distinguish whether the transient is a lensed SN or an intrinsically bright and wide class. A measurement of the source redshift via a host galaxy spectrum will be crucial to verify whether the brightness was anomalously high. DC22hxfpz shows consistent SALT2 parameters within the distribution of cosmologically normal SNe Ia ($x_1 = 1.8 \pm 0.3$), hence, we do not suspect it is a lensed SN, though in this case as well, as verification of the photometric redshift via a host galaxy spectrum will be useful to confirm whether the object was brighter than the distribution for normal SNe Ia. We note that if the bright peak magnitude is confirmed for the objects with small photo- z errors, they could also be intrinsically luminous transients, e.g. superluminous supernovae (Chen et al. 2023).

3.8 Candidates Without Static-Sky Matches

As described in Section 2.4, 137 candidates were not matched to an object in the DESI Legacy Imaging Survey Tractor catalog. Of these, 86 were only detected on a single night and were probably asteroids or flaring stars; these were not investigated further in this work. For the 51 unmatched candidates with multi-epoch photometry, we visually reviewed the color image stamps from the Legacy Survey. Of them, 14 had an object within $\sim 10''$ which *could* have been associated with the candidate, if it was a transient highly offset from its host (or if there had been an astrometry error). One candidate had a small faint object right at its coordinates, DC24kioi, the light curve for which appears to be variable (non-transient) and so is likely an AGN. The remaining 36 unmatched candidates had no discernible static-sky counterpart.

As a side note, three of 51 unmatched candidates met the initial light curve constraints to be considered potential SN Ia in Section 3.5: DC21dglus, DC21mjrj, and DC23jsner. Of the three, only DC23jsner met the more strict light curve parameter cuts to be fit with a SN Ia template, and it was also the only one of the three for which visual review revealed a faint object nearby (within a few arcseconds) which could be the host galaxy. None of the other unmatched candidates met the constraints to be considered potential SNe or fast transients.

3.8.1 Cross-match to external catalogs

The Vizier service (Ochsenbein et al. 2000) was used to cross match the 137 unmatched candidates against three catalogs: SDSS DR16 (Ahumada et al. 2020), Transiting Exoplanet Survey Satellite (TESS) Input Catalog v8.2 (Paegert et al. 2021), and SIMBAD (Wenger et al. 2000). The cross match for all three catalogs was conducted using a search radius of $5''$.

Of the 137 unmatched candidates, 31 were matched with objects in the SIMBAD catalog. All but one of these were in the COSMOS field, and mostly matched to faint, high-redshift galaxies or AGN in the deep catalogs that have been published for COSMOS (e.g., Capak et al. 2007). The one candidate in ELAIS, DC22ibvrq, was found to have a bright nearby point-source when the Legacy Survey stamp was reviewed, and was matched to a QSO published by Tie et al. (2017).

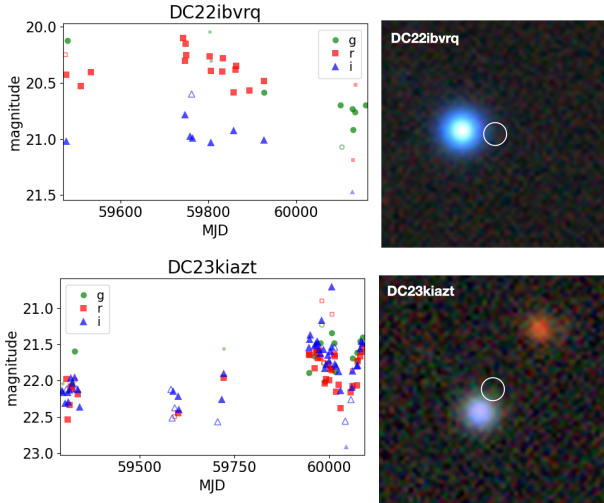


Figure 18. Unmatched candidates DC22ibvrq and DC23kiazt flagged as stars in the TESS Input Catalog v8.2, but also cross-matched to a QSO and AGN, respectively.

From the cross match with the SDSS DR16 catalog, 13 were matched with objects, all of them were in the COSMOS field as the ELAIS field was too far south for SDSS. The matches were mostly with faint, extended SDSS objects, except for DC23kiazt which was matched with a $g \sim 20$ th magnitude point source. The light curve of DC23kiazt appears to be variable (non-transient; Figure 18), and it was one of the candidates cross matched with SIMBAD to an AGN identified by Gaia (Gaia Collaboration 2020).

A cross match with the TESS catalog yielded 3 matches, candidates DC22ibvrq, DC23jqqs, and DC23kiazt, all of which were identified in the TESS catalog as stars. DC23jqqs had only a single epoch of photometry, but the light curves for DC22ibvrq and DC23kiazt are shown in Figure 18. DC22ibvrq possesses a TESS luminosity class flag as a dwarf, and based on Figure 18 it does appear to be a variable star (or QSO, based on the SIMBAD cross match) for which our absolute astrometry is slightly off. As discussed in the paragraphs above, DC23kiazt was also cross matched to an AGN in SIMBAD.

In summary, despite astrometric errors causing erroneous identifications of "unmatched" candidates in a few cases, we find that the majority of the DECam DDF's multi-epoch candidates which were unmatched to a static-sky counterpart could be associated with high-redshift galaxies (at least, this is the case in the COSMOS field, where deep legacy catalogs exist). A full analysis of what type of phenomena these candidates might be is left for future work, as here we sought only to characterize the environments of initially unmatched candidates.

4 CONCLUSIONS AND FUTURE WORK

The main message of this analysis is that there is an abundance of scientific opportunity in the 2,020 candidate light curves which are now publicly available (see Section 2.1 for access information). All are welcome to make use of these data. The main challenges that we find are that the simple methods used here to identify *potential* transients and variable stars based on the photometry alone are not satisfying, and that a comprehensive photometric classification process is needed. This work is in progress, but the lack of obvious training sets for light curves with the depth and cadence of the survey might be an issue. Scientific analysis of the DECam DDF would also benefit

from having the pipelines retain objects with *negative* difference-image fluxes, and produce direct-image magnitudes as well. This is especially useful for the analysis of non-transient events like AGN and variable stars. The LSST time-domain data products will include these kinds of measurements.

Of the transients that were classified as AGN or variable stars through cross-matching with DESI spectra, we will extract more detailed light curves without the use of difference imaging in order to get more accurate flux measurements and power spectra. We will use both aperture and PSF photometry methods for this, as well as a new technique for scene modeling of transient sources that is currently being built into the *scarlet2* package (Sampson et al. 2024). This computationally improved method for time-domain scene modeling could prove to be more accurate in generating light-curves, which would give us an improved set of reduced data for studying supernova physics and cosmology using DECAT-DDF and, eventually, LSST.

At the time of writing, the DECam DDF was due to restart observations and alert production during the 2024A semester. We plan to continue observations with the same three-night cadence (when possible). Whenever observing constraints will permit, will plan to also split some of the observations in the same night into two batches, spaced by a few hours, to allow for detection of very fast transient and variable signals. For example, as recommended by Bianco et al. (2019) for Rubin Observatory's LSST, intra-night images separated by >1.5 hours are desirable for detecting evolution in transient light curves within a night. In this DECam DDF, only 13% of our individual images were separated by >90 minutes, and as expected we found this insufficient for detecting intra-night evolution.

In addition, a new, more robust pipeline is currently under development, which will produce more consistent results, based on improved subtraction algorithms and uniform reference images. The new pipeline is planned to also include new products such as detection of negative transients (e.g., dimming of variables and AGN) and nightly stacks. Forced photometry in all difference- and direct-images, at the location of all candidates, is left as a stretch goal for future work. Finally, we intend to publish the lightcurves of transients and variables along with value-added metadata, such as cross matches to established catalogs, redshifts when available (for extra galactic sources), mean colors and magnitudes of the objects (for variables) and summary statistics such as rise time and maximum magnitude, in a database that is searchable and easy to access. Until that time, all of the data presented in this work is available via GitHub (Section 2.1) or by contacting the authors.

ACKNOWLEDGEMENTS

This DECam program for Deep Drilling Fields is a founding member of the DECam Alliance for Transients (DECAT), a logistical solution for a heterogenous group of programs all doing time-domain astronomy on a classically-scheduled telescope. Within DECAT, multiple DECam programs request that their awarded time be co-scheduled on the Blanco 4m telescope, and then the PIs work together to ensure the targets for all programs are optimally observed, and all program participants share in the observing responsibilities. We thank all NOIRLab and Blanco staff for their flexibility and support in helping to co-schedule all DECAT programs.

The DECAT nightly observing plans were primarily generated by Gautham Narayan, Dillon Brout, and Armin Rest. DECAT observers during 2021, 2022, and 2023 were Alejandro Clocchiatti, Alex Gagliano, Alfredo Zenteno, Alice Eltvéd, Amanda Wasserman, Antonella Palmese, Armin Rest, Ben Boyd, Brendan O'Connor, Chris

Lidman, Clara Martinez-Vazquez, Colin Burke, Damián Pacheco, Dillon Brout, Divya Mishra, Elana Urbach, Gautham Narayan, Guillermo Damke, Guy Nir, Haille Perkins, Igor Andreoni, Jan Kleyna, Jiawen Yang, Julio Carballo-Bello, Justin Pierel, Kathy Vivas, Keerthi Kunnumkai, Kevin Luhman, Lauren Aldoroty, Maggie Verrico, Matt Grayling, Melissa Graham, Monika Soraisam, Nicole Kane, Noor Ali, Qian Yang, Qinan Wang, Ryan Ridden-Harper, Sammy Sharief, Sasha Brownsberger, Scott Sheppard, Segev Ben-Zvi, Shenming Fu, Tom Shanks, Tomas Cabrera, Tony Chen, Ved Shah, Zach Stone, and Zhefu Yu.

This research used resources of the National Energy Research Scientific Computing Center, a DOE Office of Science User Facility supported by the Office of Science of the U.S. Department of Energy under Contract No. DE-AC02-05CH11231 using NERSC award ERCAP0024621. P.E.N. acknowledges support from the DOE under grant DE-AC02-05CH11231, Analytical Modeling for Extreme-Scale Computing Environments. LBNL is managed by the Regents of the University of California under contract to the U.S. Department of Energy.

This research uses services or data provided by the Astro Data Lab at NSF's National Optical-Infrared Astronomy Research Laboratory (NOIRLab). Based on observations at Cerro Tololo Inter-American Observatory, NSF's NOIRLab (NOIRLab Prop. IDs 2021A-0113, 2021B-0149, 2022A-724693, and 2022B-762878 under PI M. L. Graham, and 2023A-716082 under PI G. Nir). NOIRLab is operated by the Association of Universities for Research in Astronomy (AURA), Inc. under a cooperative agreement with the National Science Foundation.

The Legacy Surveys consist of three individual and complementary projects: the Dark Energy Camera Legacy Survey (DECaLS; Proposal ID #2014B-0404; PIs: David Schlegel and Arjun Dey), the Beijing-Arizona Sky Survey (BASS; NOAO Prop. ID #2015A-0801; PIs: Zhou Xu and Xiaohui Fan), and the Mayall z-band Legacy Survey (MzLS; Prop. ID #2016A-0453; PI: Arjun Dey). DECaLS, BASS and MzLS together include data obtained, respectively, at the Blanco telescope, Cerro Tololo Inter-American Observatory, NSF's NOIRLab; the Bok telescope, Steward Observatory, University of Arizona; and the Mayall telescope, Kitt Peak National Observatory, NOIRLab. Pipeline processing and analyses of the data were supported by NOIRLab and the Lawrence Berkeley National Laboratory (LBNL). The Legacy Surveys project is honored to be permitted to conduct astronomical research on Iolkam Du'ag (Kitt Peak), a mountain with particular significance to the Tohono O'odham Nation.

The Legacy Survey team makes use of data products from the Near-Earth Object Wide-field Infrared Survey Explorer (NEOWISE), which is a project of the Jet Propulsion Laboratory/California Institute of Technology. NEOWISE is funded by the National Aeronautics and Space Administration.

This project used data obtained with the Dark Energy Camera (DECam), which was constructed by the Dark Energy Survey (DES) collaboration. Funding for the DES Projects has been provided by the U.S. Department of Energy, the U.S. National Science Foundation, the Ministry of Science and Education of Spain, the Science and Technology Facilities Council of the United Kingdom, the Higher Education Funding Council for England, the National Center for Supercomputing Applications at the University of Illinois at Urbana-Champaign, the Kavli Institute of Cosmological Physics at the University of Chicago, Center for Cosmology and Astro-Particle Physics at the Ohio State University, the Mitchell Institute for Fundamental Physics and Astronomy at Texas A&M University, Financiadora de Estudos e Projetos, Fundacao Carlos Chagas Filho de Amparo, Financiadora de Estudos e Projetos, Fundacao Carlos Chagas Filho

de Amparo a Pesquisa do Estado do Rio de Janeiro, Conselho Nacional de Desenvolvimento Científico e Tecnológico and the Ministerio da Ciencia, Tecnologia e Inovacao, the Deutsche Forschungsgemeinschaft and the Collaborating Institutions in the Dark Energy Survey. The Collaborating Institutions are Argonne National Laboratory, the University of California at Santa Cruz, the University of Cambridge, Centro de Investigaciones Energeticas, Medioambientales y Tecnologicas-Madrid, the University of Chicago, University College London, the DES-Brazil Consortium, the University of Edinburgh, the Eidgenossische Technische Hochschule (ETH) Zurich, Fermi National Accelerator Laboratory, the University of Illinois at Urbana-Champaign, the Institut de Ciencies de l'Espai (IEEC/CSIC), the Institut de Fisica d'Altes Energies, Lawrence Berkeley National Laboratory, the Ludwig Maximilians Universitat Munchen and the associated Excellence Cluster Universe, the University of Michigan, NSF's NOIRLab, the University of Nottingham, the Ohio State University, the University of Pennsylvania, the University of Portsmouth, SLAC National Accelerator Laboratory, Stanford University, the University of Sussex, and Texas A&M University.

This research has made use of the SIMBAD database, operated at CDS, Strasbourg, France.

The Legacy Surveys imaging of the DESI footprint is supported by the Director, Office of Science, Office of High Energy Physics of the U.S. Department of Energy under Contract No. DE-AC02-05CH1123, by the National Energy Research Scientific Computing Center, a DOE Office of Science User Facility under the same contract; and by the U.S. National Science Foundation, Division of Astronomical Sciences under Contract No. AST-0950945 to NOAO.

DATA AVAILABILITY

See Section 2.1 for a description and links to the original images and derived photometry.

REFERENCES

- Ahumada R., et al., 2020, *ApJS*, **249**, 3
 Anderson J. P., et al., 2014, *ApJ*, **786**, 67
 Arcavi I., et al., 2012, *ApJ*, **756**, L30
 Arendse N., et al., 2023, *arXiv e-prints*, p. arXiv:2312.04621
 Astier P., et al., 2006, *A&A*, **447**, 31
 Barbary K., et al., 2023, *SNCosmo*, doi:10.5281/zenodo.8393360, <https://doi.org/10.5281/zenodo.8393360>
 Barris B. J., et al., 2004, *ApJ*, **602**, 571
 Berta S., et al., 2006, *A&A*, **451**, 881
 Bianco F. B., et al., 2019, *PASP*, **131**, 068002
 Bianco F. B., et al., 2022, *ApJS*, **258**, 1
 Blakeslee J. P., et al., 2003, *ApJ*, **589**, 693
 Boone K., 2021, *AJ*, **162**, 275
 Cackett E. M., Bentz M. C., Kara E., 2021, *iScience*, **24**, 102557
 Capak P., et al., 2007, *ApJS*, **172**, 99
 Charalampopoulos P., Pursiainen M., Leloudas G., Arcavi I., Newsome M., Schulze S., Burke J., Nicholl M., 2023, *A&A*, **673**, A95
 Chen Z. H., et al., 2023, *ApJ*, **943**, 41
 Conley A., et al., 2006, *AJ*, **132**, 1707
 Cowperthwaite P. S., et al., 2017, *ApJ*, **848**, L17
 DESI Collaboration et al., 2023, *arXiv e-prints*, p. arXiv:2306.06308
 DePoy D. L., et al., 2008, in McLean I. S., Casali M. M., eds, Society of Photo-Optical Instrumentation Engineers (SPIE) Conference Series Vol. 7014, Ground-based and Airborne Instrumentation for Astronomy II. p. 70140E, doi:10.1117/12.789466
 Dey A., et al., 2019, *AJ*, **157**, 168
 Dimitriadis G., et al., 2019, *ApJ*, **870**, L1

- Drout M. R., et al., 2014, *ApJ*, 794, 23
- Firth R. E., et al., 2015, *MNRAS*, 446, 3895
- Gaia Collaboration 2020, VizieR Online Data Catalog: Gaia EDR3 (Gaia Collaboration, 2020), VizieR On-line Data Catalog: I/350. Originally published in: 2021A&A...649A...1G; doi:10.5270/esa-lug, doi:10.26093/cds/vizieer.1350
- Gal-Yam A., 2019, *ARA&A*, 57, 305
- Garnavich P., et al., 2023, *ApJ*, 953, 35
- Gezari S., et al., 2012, *Nature*, 485, 217
- Goldstein D. A., Nugent P. E., 2017, *ApJ*, 834, L5
- Goldstein D. A., Nugent P. E., Goobar A., 2019a, *ApJS*, 243, 6
- Goldstein D. A., et al., 2019b, *ApJ*, 881, L7
- Goobar A., et al., 2017, *Science*, 356, 291
- Goobar A., et al., 2023, *Nature Astronomy*, 7, 1137
- Graham M. L., et al., 2014, *ApJ*, 787, 163
- Graham M. L., et al., 2023, *MNRAS*, 519, 3881
- Griffith R. L., et al., 2012, *ApJS*, 200, 9
- Gris P., Awan H., Becker M. R., Lin H., Gawiser E., Jha S. W., 2024, *arXiv e-prints*, p. arXiv:2405.10781
- Guy J., et al., 2007, *A&A*, 466, 11
- Hicken M., Wood-Vasey W. M., Blondin S., Challis P., Jha S., Kelly P. L., Rest A., Kirshner R. P., 2009, *ApJ*, 700, 1097
- Hillier D. J., Dessart L., 2019, *A&A*, 631, A8
- Holoien T. W. S., et al., 2014, *MNRAS*, 445, 3263
- Hosseinzadeh G., et al., 2017, *ApJ*, 845, L11
- Hung T., et al., 2017, *ApJ*, 842, 29
- Ivezić Ž., et al., 2019, *ApJ*, 873, 111
- Kasen D., 2010, *ApJ*, 708, 1025
- Kessler R., et al., 2015, *AJ*, 150, 172
- Lacy M., et al., 2013, *ApJS*, 208, 24
- Laigle C., et al., 2016, *ApJS*, 224, 24
- Li W., et al., 2011, *MNRAS*, 412, 1441
- Mauerhan J. C., et al., 2013, *MNRAS*, 430, 1801
- Nugent P., Kim A., Perlmutter S., 2002, *PASP*, 114, 803
- Ochsenbein F., Bauer P., Marcout J., 2000, *A&AS*, 143, 23
- Paegert M., Stassun K. G., Collins K. A., Pepper J., Torres G., Jenkins J., Twicken J. D., Latham D. W., 2021, *arXiv e-prints*, p. arXiv:2108.04778
- Pastorello A., et al., 2013, *ApJ*, 767, 1
- Pierel J. R., Rodney S. A., 2019, SNTD: Supernova Time Delays, Astrophysics Source Code Library, record ascl:1902.001
- Piro A. L., Morozova V. S., 2016, *ApJ*, 826, 96
- Poznanski D., et al., 2007, *MNRAS*, 382, 1169
- Quimby R. M., Aldering G., Wheeler J. C., Höflich P., Akerlof C. W., Rykoff E. S., 2007, *ApJ*, 668, L99
- Riess A. G., et al., 1999, *AJ*, 118, 2675
- Rollins M., Graham M., Knop R., Kennedy T., Nugent P., 2023, in American Astronomical Society Meeting Abstracts. p. 107.09
- Sampson M. L., Melchior P., Ward C., Birmingham S., 2024, Score-matching neural networks for improved multi-band source separation (*arXiv:2401.07313*)
- Sanders N. E., et al., 2015, *ApJ*, 799, 208
- Sarajedini V. L., Gilliland R. L., Kasm C., 2003, *ApJ*, 599, 173
- Schlegel D. J., Finkbeiner D. P., Davis M., 1998, *ApJ*, 500, 525
- Smartt S. J., Maund J. R., Hendry M. A., Tout C. A., Gilmore G. F., Mattila S., Benn C. R., 2004, *Science*, 303, 499–503
- Strolger L.-G., Riess A. G., 2006, *AJ*, 131, 1629
- Strolger L.-G., et al., 2004, *ApJ*, 613, 200
- Sullivan M., et al., 2006, *AJ*, 131, 960
- Tie S. S., et al., 2017, *AJ*, 153, 107
- Tonry J. L., et al., 2012, *ApJ*, 745, 42
- Tonry J. L., et al., 2018, *PASP*, 130, 064505
- Tonry J., et al., 2022, Transient Name Server Discovery Report, 2022-3057, 1
- Vanden Berk D. E., et al., 2004, *ApJ*, 601, 692
- Wenger M., et al., 2000, *A&AS*, 143, 9
- Zhuang M.-Y., et al., 2024, *arXiv e-prints*, p. arXiv:2402.06052
- van Velzen S., Holoien T. W. S., Onori F., Hung T., Arcavi I., 2020, *Space Sci. Rev.*, 216, 124